

~~CONFIDENTIAL~~

Copy 27

058

NASA TM X-503



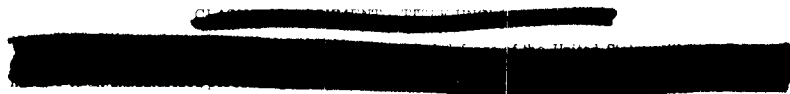
# TECHNICAL MEMORANDUM

## X-503

STEADY AND FLUCTUATING PRESSURES AT TRANSONIC  
SPEEDS ON TWO SPACE-VEHICLE PAYLOAD SHAPES

By Charles F. Coe

Ames Research Center  
Moffett Field, Calif.



DECLASSIFIED BY AUTHORITY OF NASA  
CLASSIFICATION CHANGE NOTICES NO. 7  
DATED 9-15-64 ITEM NO. 7-77A

NATIONAL AERONAUTICS AND SPACE ADMINISTRATION  
WASHINGTON

March 1961

~~CONFIDENTIAL~~

DECLASSIFIED

~~CONFIDENTIAL~~

NATIONAL AERONAUTICS AND SPACE ADMINISTRATION

TECHNICAL MEMORANDUM X-503

STEADY AND FLUCTUATING PRESSURES AT TRANSONIC  
SPEEDS ON TWO SPACE-VEHICLE PAYLOAD SHAPES\*

By Charles F. Coe

SUMMARY

Steady and fluctuating pressures have been measured at Mach numbers which were varied from 0.6 to 1.2 on two bodies of revolution typical of two space-vehicle payload shapes, the Centaur and the Able V.

The results of the investigation showed that significant fluctuations of pressure occurred on both bodies between Mach numbers of 0.75 and 1.00. The maximum fluctuations measured at any Mach number and angle of attack occurred in the region of the normal shock wave as a result of shock-wave motion. Large regions of unsteady pressure also occurred as a result of separation on the converging afterbody of the Able-V model. The maximum pressure fluctuations occurring on the bodies increased with increasing angle of attack. For angles other than  $0^\circ$ , fluctuations of normal force are indicated since pressure fluctuations were larger on the upper half of the bodies than on the lower half.

No definite conclusions could be drawn regarding the form of the spectral densities of pressure fluctuations in the region of the shock wave. The spectral densities in regions of separation following the shock wave appeared flat except for some increase in energy level below 100 cycles per second, which may have been due to slight model motions.

INTRODUCTION

Large structural loads can be encountered by an exiting space vehicle as it traverses the transonic range because dynamic pressure is near the maximum with the result that large pressure gradients occur in the presence of shock waves. Moreover, the shock waves may be unsteady so the characteristic flow instabilities associated with buffeting are present. The aerodynamic loads associated with the unsteady pressures and the large pressure gradients can impose a structural design problem which may be due to local panel loading on a space-vehicle fairing, or the excitation of the over-all vehicle structure, or even one of transmitting unsteady loads to delicate payload and guidance instruments.

\*Title, Unclassified

DECLASSIFIED BY AUTHORITY OF NASA  
CLASSIFICATION CHANGE NOTICES NO. 7-  
DATED 9-15-64 ITEM NO. 7-78

031713241030

2

~~CONFIDENTIAL~~

Results of investigations, such as reference 1, may be helpful in estimating loading due to pressure gradients, and in estimating internal venting requirements for fairings. Although some measurements of local pressure fluctuations on two-dimensional airfoils have been made (e.g., refs. 2 and 3), measurements of unsteady pressures on bodies of revolution were heretofore unavailable for consideration in the design of space vehicles.

As a consequence, an investigation was undertaken to provide measurements at transonic speeds of both steady and fluctuating pressures on typical space-vehicle shapes, and to determine whether shapes of payload stages can be optimized to give minimum unsteady loading. The general research program was under way when failure of an Able-IV moon shot occurred within the transonic speed range. The research results available suggested the possibility of fluctuating pressures on the payload fairing contributing to the failure, and led to the desirability of testing two specific vehicle shapes. These were the Centaur, which requires a jettisonable insulation that may be vulnerable to fluctuating pressures, and the Able V, which was to succeed the Able IV. It is the results of these two tests that are contained herein and, although they are for specific model shapes, it is believed that they can provide information of value for design studies.

#### NOTATION

$C_p$	time-average pressure coefficient, $\frac{p - p_o}{q_o}$
$\Delta C_p(\text{RMS})$	coefficient of the root-mean-square fluctuation of pressure about the mean
$\Delta C_p(\text{pk-to-pk})$	coefficient of the peak-to-peak fluctuation of pressure about the mean
$M$	free-stream Mach number
$D$	maximum body diameter
$p$	local static pressure
$p_o$	free-stream static pressure
$q_o$	free-stream dynamic pressure
$x$	distance along body axis from nose
$\alpha$	angle of attack

~~CONFIDENTIAL~~

DECLASSIFIED

CONFIDENTIAL

3

## APPARATUS AND TECHNIQUE

### Wind Tunnel


Tests for this investigation were conducted in the Ames 14-Foot Transonic Wind Tunnel at Mach numbers from 0.60 to about 1.20. Details of the nozzle and test section of this facility are shown in figure 1. This tunnel operates at a constant stagnation pressure, approximately atmospheric, but some control of stagnation temperature is possible. As a result, Reynolds number varies with Mach number as illustrated in figure 2. The shaded areas indicate the variation of Reynolds number, based on maximum body diameters, for each of the models tested. Flow curvature and angularity in the test section have been measured and are negligible. The Mach number is constant within  $\pm 0.005$  Mach number.

### Models

Two models were tested, a 0.074-scale Centaur having the nominal hemisphere-cone-cylinder shape without any external protuberances, and a 0.25-scale Able V. Both were tested in the presence of a cylindrical extension of approximately two body-base diameters in length. The diameter of the extension on the Centaur model was scaled to that of an Atlas booster. Sketches of the models showing pertinent dimensions and also the locations of static-pressure orifices and pressure transducers are in figure 3. Photographs of the models are in figure 4.

Both models can be considered to be of rigid construction, and were rigidly attached to the tunnel sting-support system. The model having the Centaur shape was constructed of Fiberglas braced with steel rings, whereas the model with the Able-V shape was constructed of solid wood with material removed at the core to make room for necessary pressure tubes and wires. A solid wooden nose extending back to  $x/D = 1.741$  was constructed for the Centaur model to check the effect of the Fiberglas flexibility. Shake tests of the model-support system with the Centaur model installed with the solid wooden nose indicated resonant frequencies of the over-all system of 8.8, 26.6, 46.0, 72.0, 86.3, 189, and 241 cycles per second. Except for the first, second, and third sting-bending modes at 8.8, 26.6, and 72.0, the remaining modes could not be definitely identified. Shake tests of the Able-V model indicated resonant frequencies of 10.7, 29.8, 60.5, 117, 191, and 281 cycles per second. The first five frequencies listed were identified as the first five bending modes of the support system.

The Centaur model had two longitudinal rows of both orifices and pressure transducers. Orifices were located at peripheral angles of  $0^\circ$  (top center line) and  $45^\circ$  clockwise. Since the Able-V model had only one



03712201030

4

CONFIDENTIAL

row of orifices and transducers, measurements were obtained from duplicate tests of the model with orifices set first at  $0^\circ$  and then  $45^\circ$ . The centers of the pressure transducers were offset to the right of their adjacent orifices  $3/8$  inch on the Centaur model and  $1/2$  inch on the Able-V model. These represent an angular offset of approximately  $4.75^\circ$  at the maximum diameters of both bodies. For practical purposes, the transducers will be referred to as being located along the  $0^\circ$  and  $45^\circ$  orifice rows.


#### Instrumentation

A photograph of sample pressure transducers is shown in figure 5. The transducers, which were made at Ames Research Center, were 0.250-inch diameter and 0.075 inch thick.<sup>1</sup> They were of the bonded strain-gage type having a single active leg of the strain-gage bridge mounted on the back of a thin diaphragm. The remaining three legs of the bridge, which were inactive legs, were mounted within the model in close proximity to the active leg. Calibrations of the transducers have shown them to have linear outputs over at least  $\pm 2$  pounds per square inch. To avoid exceeding this range during operation, the back side of the diaphragm on each transducer was referenced to the static pressure from an adjacent orifice. Although single-active-leg strain-gage construction results in d.c. drift in output due to temperature variations, the transducers are sufficiently insensitive to temperature effects to allow d.c. calibrations to be made for the determination of the dynamic sensitivity. The slopes of the calibration curves are also relatively unaffected by temperature. Check calibrations following manufacture of the transducers showed less than 2-percent variation in the output sensitivity between room temperature and  $160^\circ$  F. The dynamic response of the transducers was also checked by mechanically oscillating a sample transducer, and as a result the transducers are considered to have a flat response to 1000 cycles per second.

Each transducer was installed in a model by bonding the reference tube and wires on one side and the plugged dummy tube on the other side to slots on each side of its receptacle. An adhesive with a rubberlike quality was used to minimize any transmission of skin stresses to the transducer body. The reference pressure tube was brought out of the tunnel along with the tube from its adjacent static-pressure orifice, and the two were interconnected at the mercury-in-glass manometers used for recording static pressures. The long combined tube length, approximately 150 feet from the orifice to the back of the transducer diaphragm, insured the steadiness of reference pressure.

---

<sup>1</sup>One exception was a 0.500-inch-diameter pressure transducer installed in the solid wooden nose for the Centaur model as a check of the satisfactory operation of the transducers.



DECLASSIFIED

CONFIDENTIAL

5

Major electronic components used for both recording and analyzing data from each pressure transducer are shown in a block diagram in figure 6. Most of the components are standard, with the exception of the filters which affect the frequency characteristics of the data and the power-spectrum analyzer. In the data-recording circuit the high-pass filter attenuated the signal level 3 db at 1 cps at the rate of 6 db per octave. It was placed in the circuit to eliminate d.c. drift due to tunnel temperature variations so that the maximum tape-channel range was available to pressure-fluctuation signals only. In the root mean square and oscillograph recording circuit, the band-pass filters further eliminated d.c. and very low frequencies,<sup>2</sup> and also any frequencies above the linear-response range of the transducers. These were 6-db-per-octave filters which attenuated the signal 3 db at 7 and 1000 cps. The galvanometers in the oscillograph are specified by the manufacturer to have a response flat within  $\pm 5$  percent to 350 cps. The power spectrum analyzer is a beat-frequency-type instrument containing a variable sixth-order filter.


One other instrument, a vibration meter, was used for only a few test points during the Centaur model tests. The integrating circuit provided a signal proportional to displacement from a velocity pickup installed at  $x/D = 2.124$ .

#### Procedure

Calibrations of all the pressure transducers and tape recorder channels were made before each test in order to minimize the possibility of effects of small changes in sensitivity. The pressure transducers were calibrated from outside the tunnel through the reference tubes to the back side of the diaphragms. The tape recorder was calibrated with a 100 cps sine wave of known root-mean-square voltage.

The procedures for conducting the tests of the two models were slightly different. For the model with the Able-V shape, tests were conducted at selected Mach numbers from 0.60 to 1.15, and the angle of attack was varied at each Mach number from  $-6^\circ$  to  $+10^\circ$ . With this system the maximum pressure fluctuations, which occur quite locally, could have been missed. For the model with the Centaur shape, tests were conducted at constant angles of attack from  $-4^\circ$  to  $+8^\circ$ , and the Mach number was varied from 0.60 to 1.20. In the range of Mach numbers where significant pressure

<sup>2</sup>The decision to further filter low frequencies in addition to the filtering during recording was prompted by power spectral analyses of pressure fluctuation ahead of the shock wave. The results indicated that much of the peaking in the recorded spectra below 10 cps was due to either fluctuations of dynamic pressure or stream angle within the wind-tunnel test section.



CONFIDENTIAL

fluctuations were occurring ( $0.7 < M < 1$ ), the Mach number was adjusted in whatever increments were required to locate the maximum intensities at the pressure-transducer stations spaced along the top center line of the model. For each Mach number and angle-of-attack setting, a photograph was taken of a multiple mercury-in-glass manometer for the measurement of steady pressures, while a 1-minute-long tape record was taken for the measurement of unsteady pressures.

To reduce the data to determine the RMS pressure-fluctuation intensities, digital-recorder readings of the RMS voltages were taken at about 2-second intervals throughout the duration of each 1-minute record. The average of the readings was then applied to the calibrated sensitivities of the pressure transducers in terms of pounds per square foot per volt to yield the measurements of fluctuating pressure. The peak-to-peak pressure fluctuations were obtained by applying the calibrated sensitivity of the appropriate pressure transducer in terms of pounds-per-square-foot-per-inch deflection of the oscillograph trace to a visual estimate of the double amplitude of the trace during approximately a 5-second record taken from the 1-minute tape recording. Measurements of the peak-to-peak fluctuations were made only for the corresponding data points where significant RMS readings occurred.


Power-spectral analyses were performed at a band-width setting of 6 cps with a 22-second tape loop operating at the same tape-transport speed as the original recordings. The prerun 100-cps calibration signal was analyzed prior to the analysis of each of the selected test points. The known RMS voltage of the calibration signal was then related to the voltage sensitivity of the pressure transducers to establish the mean-square-pressure per-cycle-per-second scale of the recording potentiometer.

No corrections have been made to the steady pressure readings, and no attempt has been made to subtract any tare readings (with the exception of the band-pass filtering) from the fluctuating-pressure data due to either wind-tunnel or instrumentation-induced noise levels. Aside from the problem of establishing the correct part of the total signal caused by flow roughness and instrumentation noise, it was impractical to make corrections to the large number of test points with proper correlation of noise factor and unsteady pressure. An indication of the average wind-tunnel and instrumentation noise levels can be obtained from the level of the pressure-fluctuation measurements ahead of the peaks shown in figures 7 and 8.

## RESULTS AND DISCUSSION

### Pressure Fluctuations

Pressure fluctuations and their relationship to static pressures.--  
The longitudinal distributions of the intensities of the pressure



DECLASSIFIED

CONFIDENTIAL

7

A  
4  
5  
5

fluctuations are shown in figure 7 for the Centaur model and in figure 8 for the Able-V model. The distributions are presented as a function of the number of maximum body diameters back from the nose for all the Mach numbers investigated. To associate the pressure fluctuations with transonic-flow phenomena, such as the presence of shock waves, their strength and locations, etc., some of the distributions of the pressure fluctuations are presented with their corresponding static-pressure distributions in figures 9 and 10. In all of these figures (figs. 7 through 10), data that were obtained at negative angles of attack are presented as reflections in the vertical plane at positive angles of attack to show the effective longitudinal distributions of steady and fluctuating pressures at peripheral stations of  $135^\circ$  and  $180^\circ$ . Where it was considered that the peak in the fluctuating-pressure distribution had been missed due to its having been between transducer stations for the particular Mach number setting, representative peaks have been faired with dashed lines to indicate their approximate locations.

Examination of figures 7 and 8 discloses that fluctuations of pressure occurred on both models at transonic speeds. In general, the most intense fluctuations were concentrated longitudinally at only one transducer station. On figures 9 and 10, which contain the static-pressure distributions, it can be seen that these maximum fluctuations usually appear where there is a steep rising pressure gradient through a normal shock wave. Their occurrence in the region of the shock wave is attributed to the motion of the shock wave and the consequent fore-and-aft shifting of the pressure rise.

Although the largest fluctuations of pressure on a body may be concentrated longitudinally at the shock wave, it is apparent from the results in figure 8 that large regions of unsteady flow can occur at angle of attack on a converging afterbody, such as exists on the Able V. As a matter of fact, the most notable difference between the distributions of the pressure fluctuations on the two models is that these large regions of pressure fluctuations following the shock wave did not occur on the Centaur model. Figure 11, which pictures the flow over a portion of each model for a few Mach numbers and angles of attack, shows that separation was more extensive on the upper surface of the Able-V model. These results indicate that there is a danger that a large area may become exposed to unsteady pressures on a space vehicle if the payload fairing is larger in diameter than its adjacent rocket stage.

Effects of Mach number and angle of attack on maximum pressure fluctuations.- The maximum fluctuations measured along the top center line of the models have been plotted versus Mach number in figure 12 to show in a more consolidated form the magnitude of the maximum fluctuations, the range of Mach numbers where large fluctuations occurred, and the effect of angle of attack. Curves are faired through the points plotted at constant angle of attack for the Centaur model, but are omitted for the Able-V model because of the uncertainty that the maximum fluctuations

[REDACTED]



03:41:29.1030

CONFIDENTIAL

8

were measured at every test Mach number. The data show that the significant fluctuations occurred on both models at Mach numbers above 0.75 and below 1.0. Maximum intensities of the fluctuations of pressure coefficient reached values of 0.106 on the Centaur model and 0.124 on the Able-V model. It is possible that the range of Mach numbers for flow unsteadiness may vary for certain body shapes where subsonic separation could become a factor (ref. 1). However, the fact that the largest fluctuations occurred at the locations of normal shock waves suggests that for most shapes the problem area in connection with unsteady pressures will be within the same Mach number range.


The effect of increasing angle of attack on the maximum fluctuations, as shown by the results from the Centaur model in figure 12, was generally to increase the intensities.

Relationship between peak-to-peak and RMS measurements.-- Although peak-to-peak measurements are of little statistical value, they are of interest from the standpoint of examining the maximum instantaneous pressure fluctuations that may occur. To indicate how large the peak-to-peak fluctuations of pressure may become in relation to RMS fluctuations, peak-to-peak values of pressure coefficient are plotted in figure 13 against corresponding RMS values that exceeded 0.01. The results indicate that the ratios between the peak-to-peak and RMS measurements, although somewhat scattered, are sufficiently consistent to provide a reasonable means of estimating maximum peak-to-peak values from RMS readings or vice versa. The peak-to-peak fluctuations were from about three to four times higher than their corresponding RMS measurements for the Centaur model (fig. 13(a)), and from about three to five times higher for the Able-V model (fig. 13(b)).

Figure 13 also shows that the maximum coefficient of peak-to-peak fluctuations of pressure measured within the range of this investigation reached values of 0.355 on the Centaur model and 0.428 on the Able-V model. At the dynamic-pressure levels of the test these measurements correspond, respectively, to unsteady pressures of 222 and 334 pounds per square foot.

Power spectral densities.-- Before experimentally determined pressure fluctuations can be applied in calculations to determine the response of a structure, properties of the fluctuations other than the RMS intensities must be either evaluated from the test results or estimated. Probably the most important of these is the power spectral density, which represents the variation with frequency of the mean-square value of the amplitude of the pressure fluctuations. It is also necessary to establish from the power spectra, if possible, whether the results are representative of the input function and not influenced by the model-installation dynamics.

Spectral densities that are typical of the two types of pressure fluctuations measured during this investigation are shown in figures 14



DECLASSIFIED

CONFIDENTIAL

9

and 15. Fluctuations which occurred at the locations of the shock waves on both models are represented in figure 14, while fluctuations within regions of separation, which were of consequence only on the Able-V model, are represented in figure 15. Also indicated in figure 14(a) is a spectrum from the repeat test to determine the effect of Fiberglas flexibility on the Centaur, and the repeatability of the pressure-fluctuation measurements with a 1/2-inch-diameter transducer. The results show that the spectral densities at the same Mach number and angle of attack were essentially the same.<sup>3</sup>

Examination of figure 14 discloses that peaks in the spectral density occurred near one or more of the model resonant frequencies. These results suggest some coupling of shock-wave motion with vibration modes of the model-support system. Since there was no measurable amplitude of motion (fig. 16) at 192 cps, the question is raised as to the cause of the peak shown at 192 cps in the spectral densities for  $x/D = 1.634$  on the Centaur model and  $x/D = 0.800$  on the Able-V model. The occurrence of a peak in the spectra of the pressure fluctuations ahead of the shock wave (fig. 17) at 193 cps at  $M = 0.80$  and at 215 cps at  $M = 0.95$  indicates that a possible cause may be a very small pressure fluctuation in the stream (equivalent to less than  $0.022 \text{ psf}^2/\text{cps}$  at  $M = 0.80$ ) which varies with Mach number.

In view of the apparent influence of motion and/or stream fluctuations, a brief investigation of the pressure fluctuations on the Centaur model was conducted in the 11-foot test section of the Ames Unitary Plan Wind Tunnel. The results show that the peak at 192 cps disappeared (fig. 18), and that with the exception of the disappearance of this peak, the general distribution of the energy with frequency at  $x/D = 1.634$  was about the same. At  $x/D = 1.970$  some coupling of the pressure fluctuations with motion at low frequencies is still indicated. Although the amplitude of motion was less in the 11-foot wind tunnel (fig. 19), the RMS intensities (fig. 20) did not diminish from the original measurements shown in figure 12, a fact which helps substantiate all the RMS measurements presented.

Since coupling seems to occur between pressure fluctuations in the region of the shock wave and vehicle motion and/or stream fluctuations, a serious problem area is indicated by the extremely small motions and fluctuations required to influence the frequency distribution of the unsteady pressure. As previously pointed out an alteration of the model support properties did not change RMS measurements; consequently it appears that an effective amplification of the pressure fluctuations can take place with a redistribution of the total energy to form peaks at the frequency of motion.

<sup>3</sup>The fact that the power spectra were the same indicates that the pressure fluctuations are a stationary random function of time. That unsteady forces associated with buffeting are a stationary random function of time and the defining statistical properties of such functions are discussed to some extent in reference 4.

037120A.1030

10

CONFIDENTIAL

From the spectra of the fluctuations in the separated region following the shock wave (fig. 15), it can be seen that they were affected by model motions to a considerably lesser extent than the pressures in the region of the shock wave, and that the general shapes were about the same for all the cases shown. Except for the slight increases in energy level at frequencies from 100 cps downward to 10 cps, which may have been due to model motions, the frequency distributions were practically constant for the remaining range of frequencies. The very low levels of the spectral densities of the output from a covered transducer within the separated region and transducers located ahead of the shock wave (fig. 17) demonstrate that the major part of the flat distributions is a measure of pressure fluctuations and not of instrumentation or wind-tunnel induced noise levels.


A  
4  
6  
5

#### Steady Pressures

In general, the inside of a space-vehicle payload fairing is vented to local static pressure at some longitudinal station to minimize the loading on the fairing during launch. However, at transonic speeds pressure fluctuations and pressure gradients are large, and regions of differential loading can occur over the length of the body. Depending upon the choice of venting locations, the loading on the fairing structure can be entirely compressive or it can impose stresses which may vary longitudinally from compression to tension. The results in figure 9 show that with a shape such as the Centaur, the position of minimum pressure always occurred in the test Mach number range at the same station so that compressive loading could be maintained by venting at that location. Venting to free-stream static pressure could also be done on a shape similar to the Centaur since pressures recovered to free-stream static pressure more readily on the cylindrical afterbody than on the converging afterbody of the Able V.

#### Over-All Loads

Although the most severe localized loading would be encountered at the normal shock wave because of the combined steep static-pressure gradient and high pressure fluctuations, it would be necessary to correlate the adjacent pressure fluctuations both circumferentially and longitudinally before the over-all time-dependent part of the loading could be determined. No cross spectral densities or correlation coefficients have been obtained that would relate the pressure fluctuations at the different stations on the models tested. Assumptions could be made of the over-all loading on a shape similar to the Centaur model, however, which may be reasonably valid in view of the fact that all significant fluctuations were concentrated at the location of the shock wave. First, it would seem reasonable



DECLASSIFIED

CONFIDENTIAL

11

that the longitudinal correlation could be ignored. Then for circumferential correlation, it could be assumed that the shock wave surrounding the body fluctuates with all peripheral stations in phase.

In general, the loading due to steady and fluctuating pressures has been considered from the point of view of panel loading. In addition, normal-force and side-force fluctuations, which are the summation of the components of local pressure fluctuations in the normal-force and side-force planes, can cause dynamic response of the vehicle. The fact that large areas may be exposed to unsteady pressures in regions of separation indicates that the normal forces can be unsteady. Normal-force fluctuations are indicated by the results of figures 7(b), 8(b), and 8(c) which show that for angles of attack other than  $0^\circ$  where pressure fluctuations were significant, they were larger on the upper half of the bodies than on the lower half.

### CONCLUSIONS

The measurements of steady and fluctuating pressures at transonic speeds on two bodies of revolution (Centaur and Able-V shapes) have shown the following:

1. Significant fluctuations of pressure coefficient occurred on both bodies within the Mach number range from 0.75 to 1.00. The highest root-mean-square intensities measured were 0.106 (0.355 peak-to-peak) on the Centaur model and 0.124 (0.428 peak-to-peak) on the Able-V model.
2. The maximum fluctuations measured at any Mach number and angle of attack occurred in the region of the shock wave.
3. On the converging afterbody of the Able-V model, large regions of unsteady pressures occurred in the separated flow behind the shock wave at angle of attack.
4. Maximum pressure fluctuations occurring on the bodies increased with increasing angle of attack within the range of angles investigated.
5. Pressure fluctuations were generally larger on the upper half of the bodies than on the lower half at angles of attack greater than  $0^\circ$ , indicating that appreciable fluctuations of normal force were also acting on the bodies.

0371204 1034

12

CONFIDENTIAL

6. Except for some increase in energy level below 100 cps, which may have been due to slight model motions, the spectral densities of pressure fluctuations in regions of separation following the shock wave appeared flat over the range of frequencies examined.

Ames Research Center

National Aeronautics and Space Administration

Moffett Field, Calif., Jan. 27, 1961

#### REFERENCES

1. Cleary, Joseph W.: The Effects of Nose Bluntness on the Flow Separation and Longitudinal Characteristics of Ellipsoidal-Nosed Cylinder-Flare Models at Transonic Speeds. NASA TM X-370, 1960.
2. Coe, Charles F.: A Study of Local-Pressure Fluctuations Relative to Static-Pressure Distributions on Two-Dimensional Airfoils at High Subsonic Mach Numbers. NACA RM A55J11, 1955.
3. Humphreys, Milton D.: Pressure Pulsations on Rigid Airfoils at Transonic Speeds. NACA RM L51112, 1951.
4. Polentz, Perry P., Page, William A., and Levy, Lionel L., Jr.: The Unsteady Normal-Force Characteristics of Selected NACA Profiles at High Subsonic Mach Numbers. NACA RM A55C02, 1955.

A  
4  
6  
5

DECLASSIFIED

CONFIDENTIAL

13

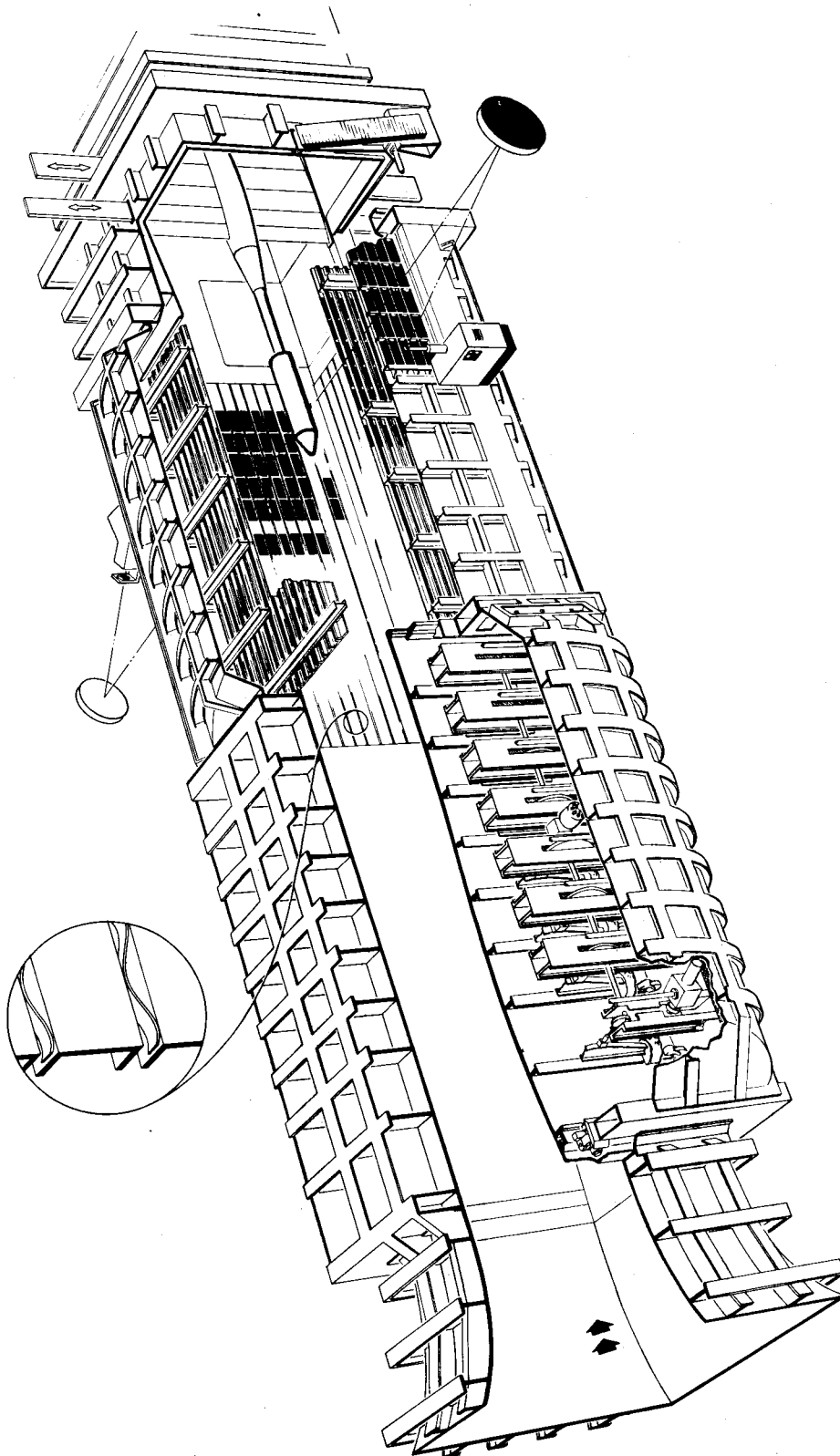


Figure 1.- Nozzle and test section of the Ames 14-Foot Transonic Wind Tunnel.

A  
4  
6  
5

03171230.1030

14

CONFIDENTIAL

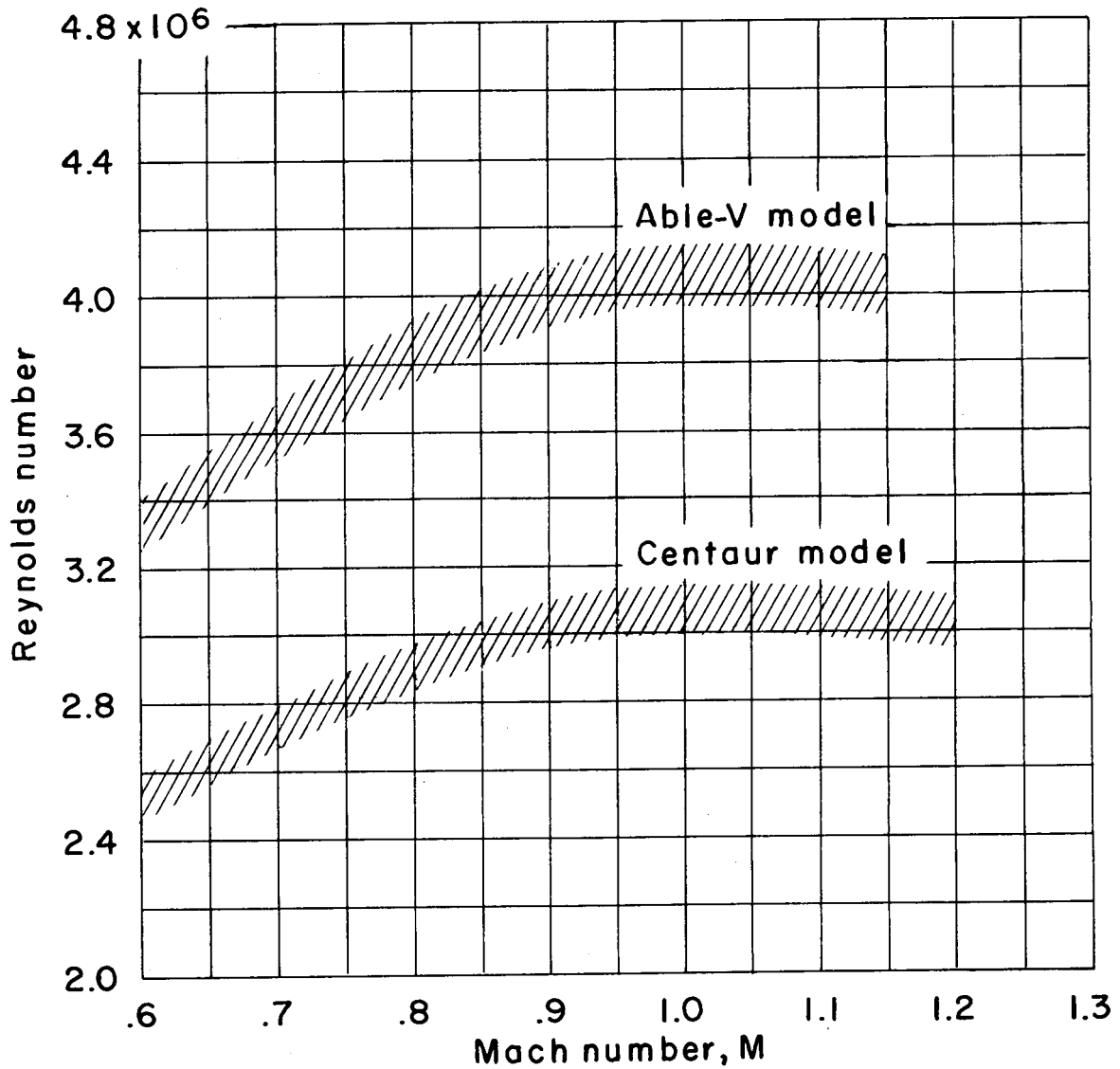
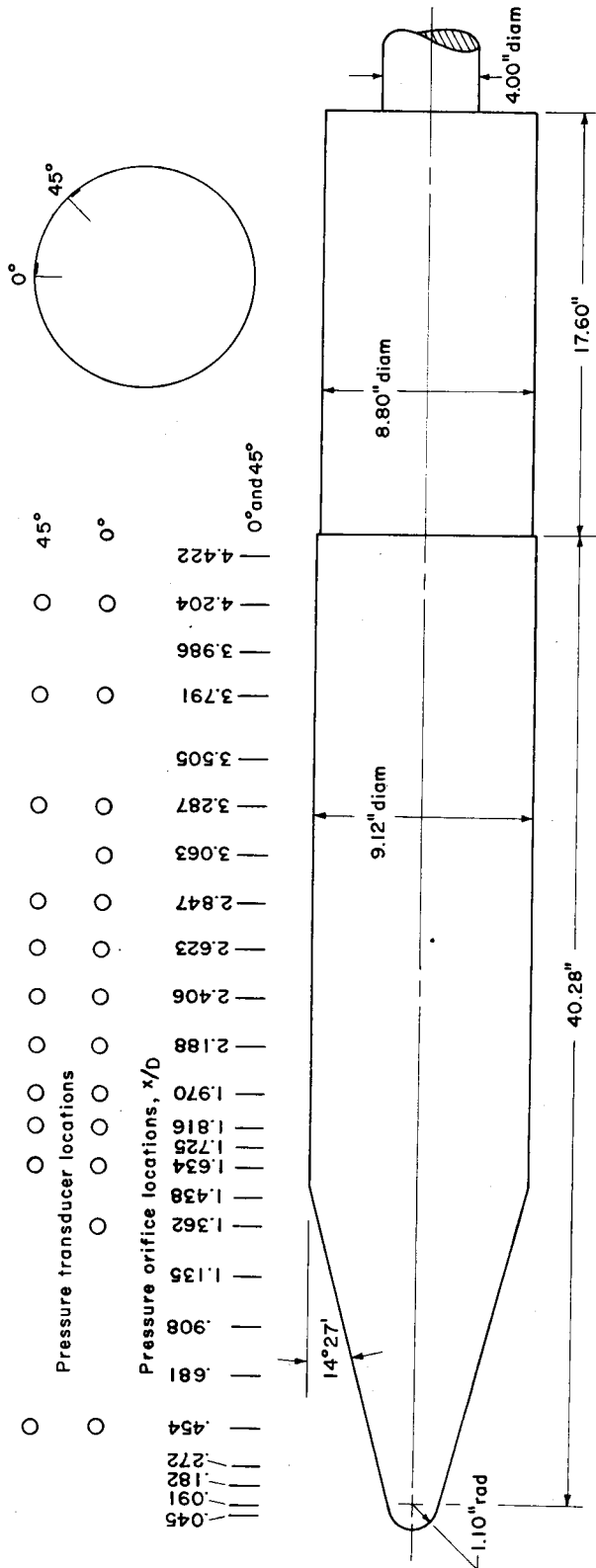


Figure 2.- Reynolds number ranges for the two models tested.



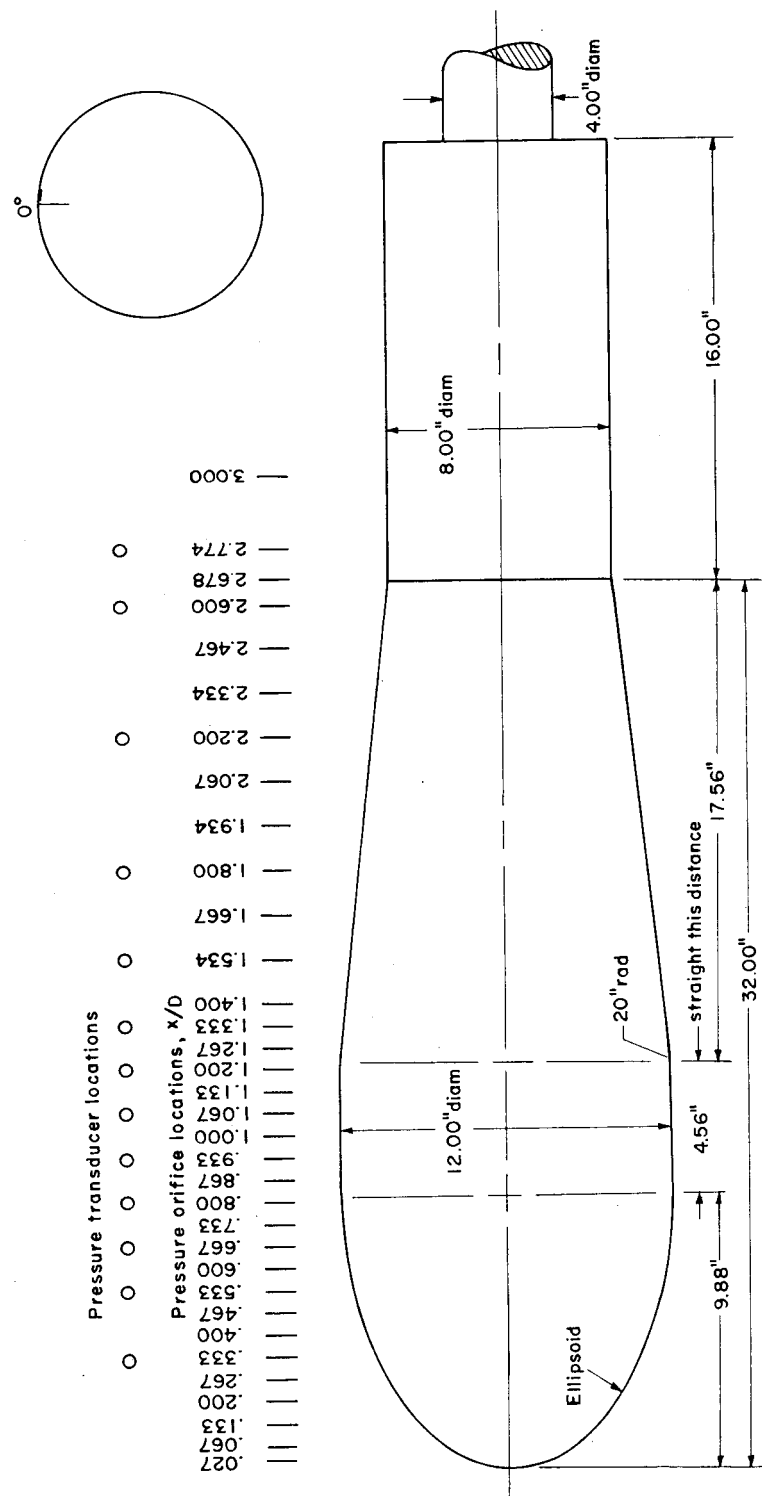
(a) Centaur model.

Figure 3.- Sketches of models showing pertinent dimensions and locations of the static-pressure orifices and pressure transducers.



037133A.030

CONFIDENTIAL



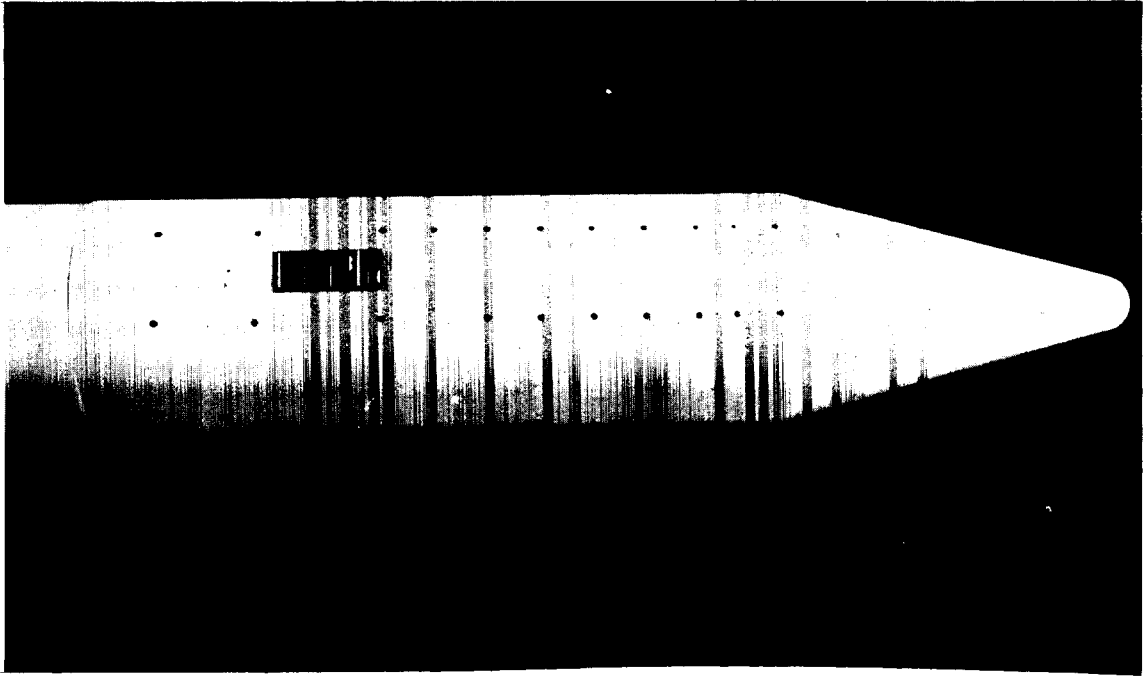
(b) Able-V model.

Figure 3.- Concluded.

DECLASSIFIED

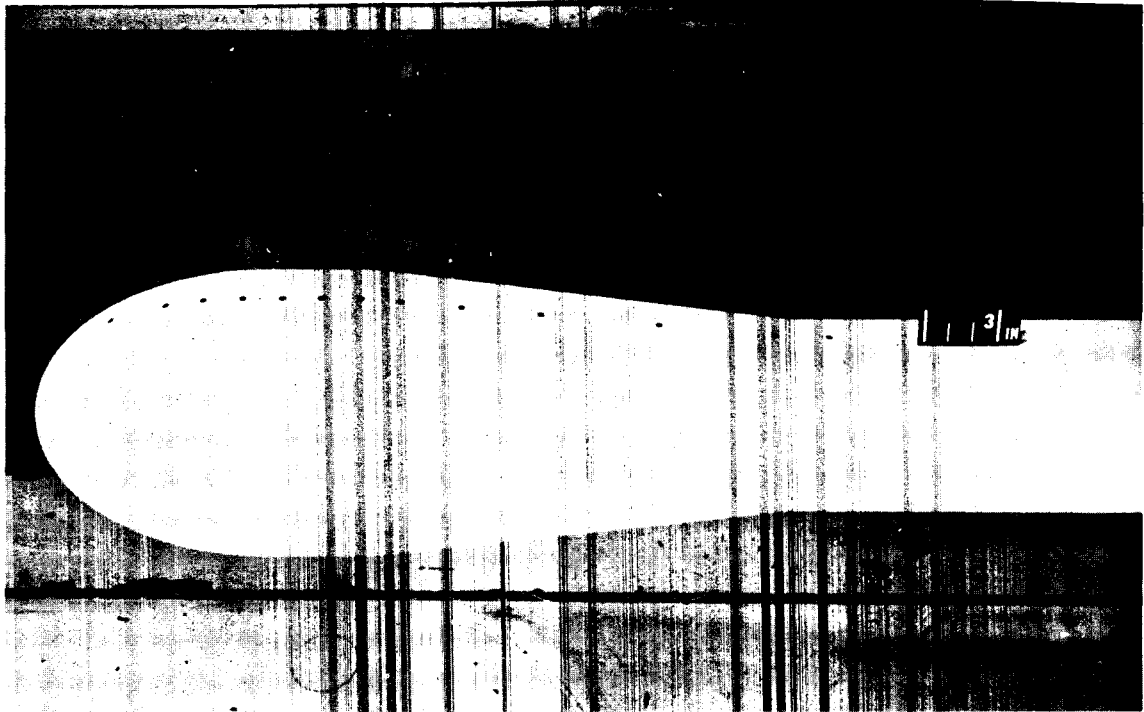
CONFIDENTIAL

17



(a) Centaur.

A-26648



(b) Able V.

A-26383

Figure 4.- Photographs of models.



037120A.D30

18

CONFIDENTIAL

A-24683

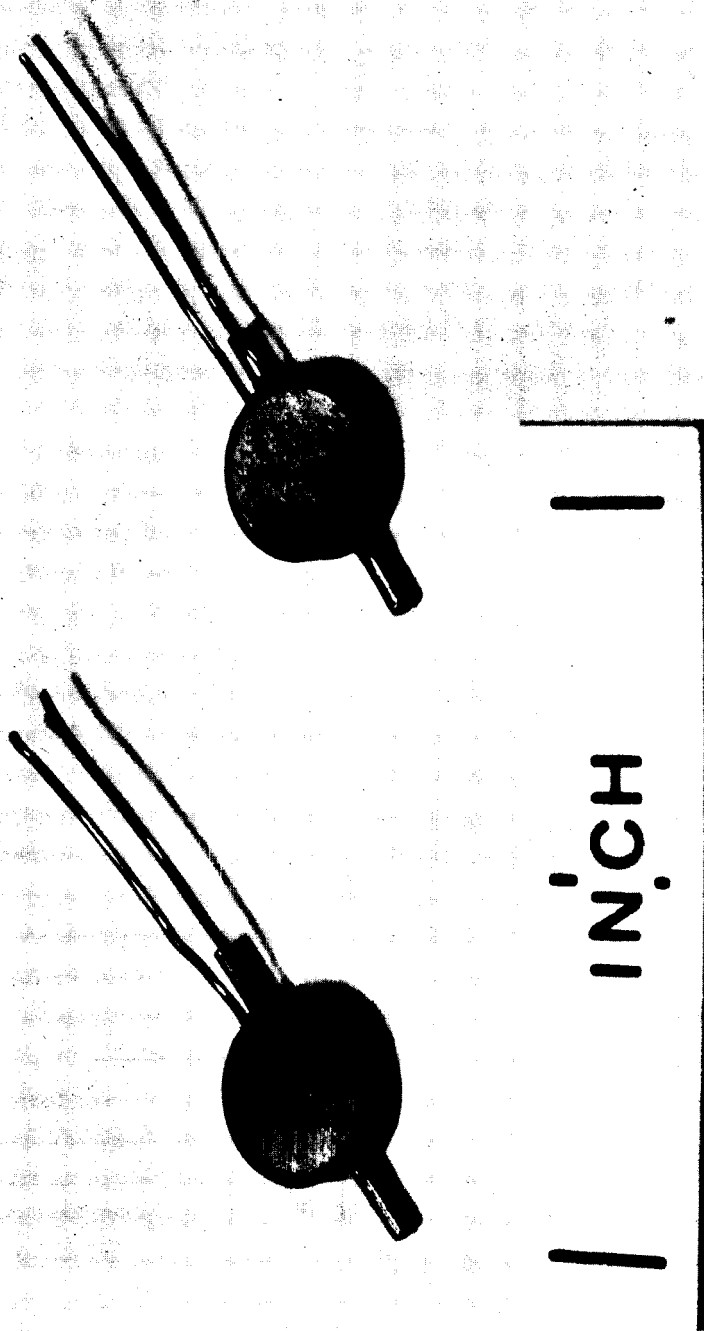


Figure 5.- Photograph of sample pressure transducers.

DECLASSIFIED

CONFIDENTIAL

19

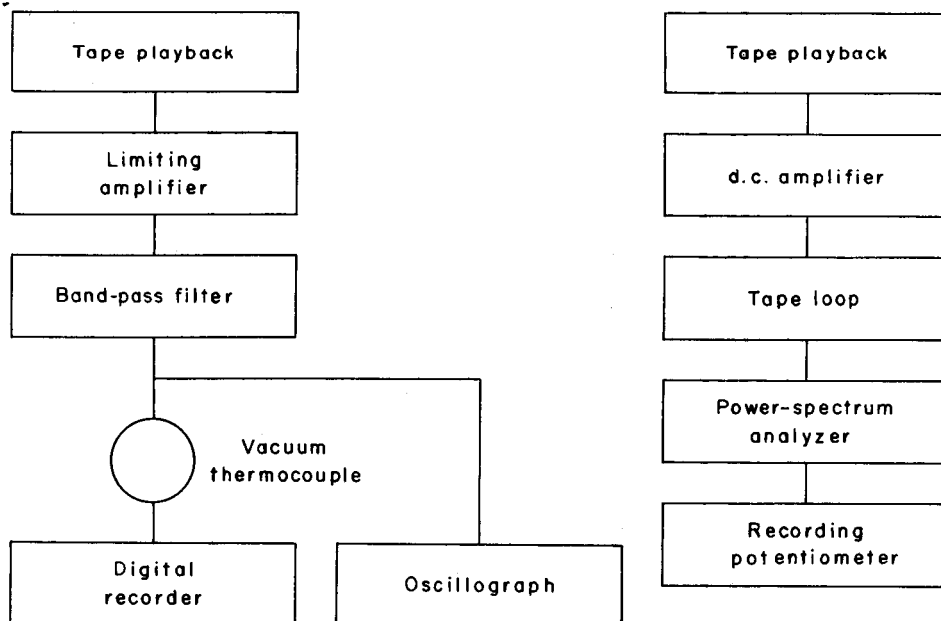
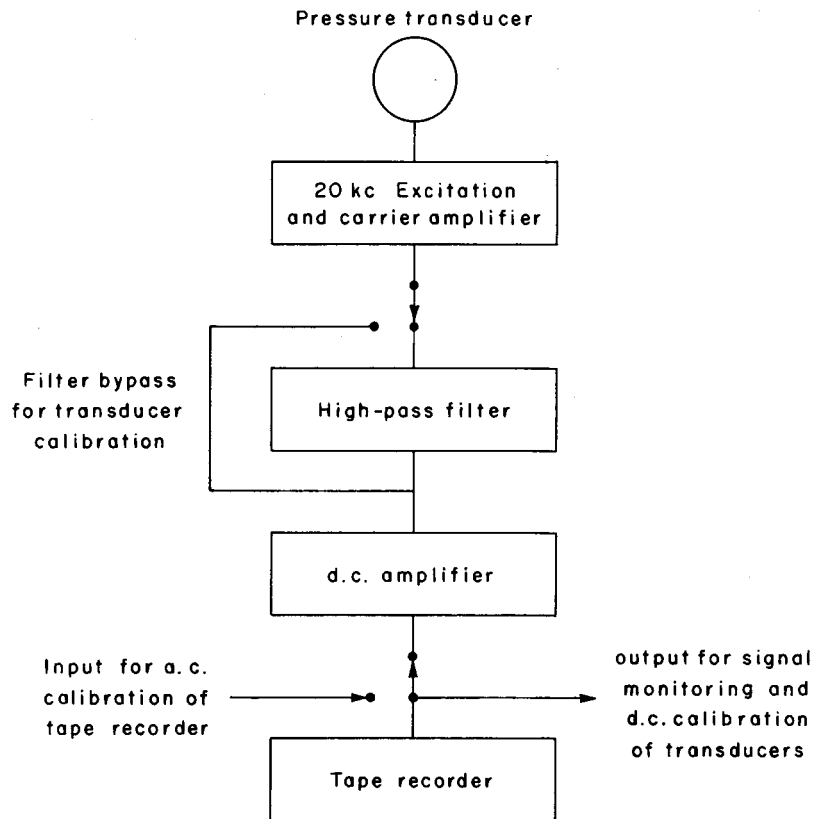
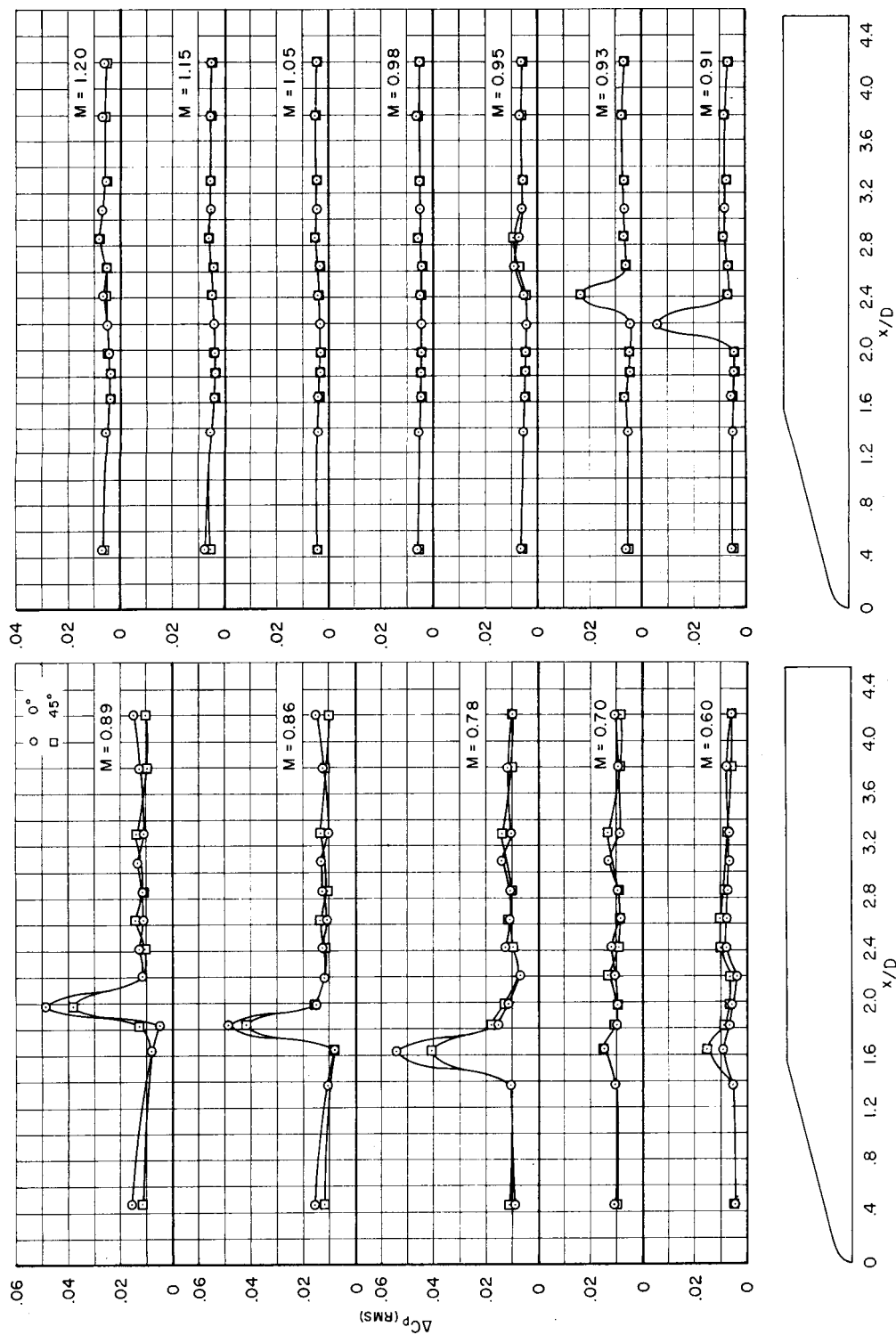


Figure 6.- Block diagram of major components of instrumentation.

CONFIDENTIAL



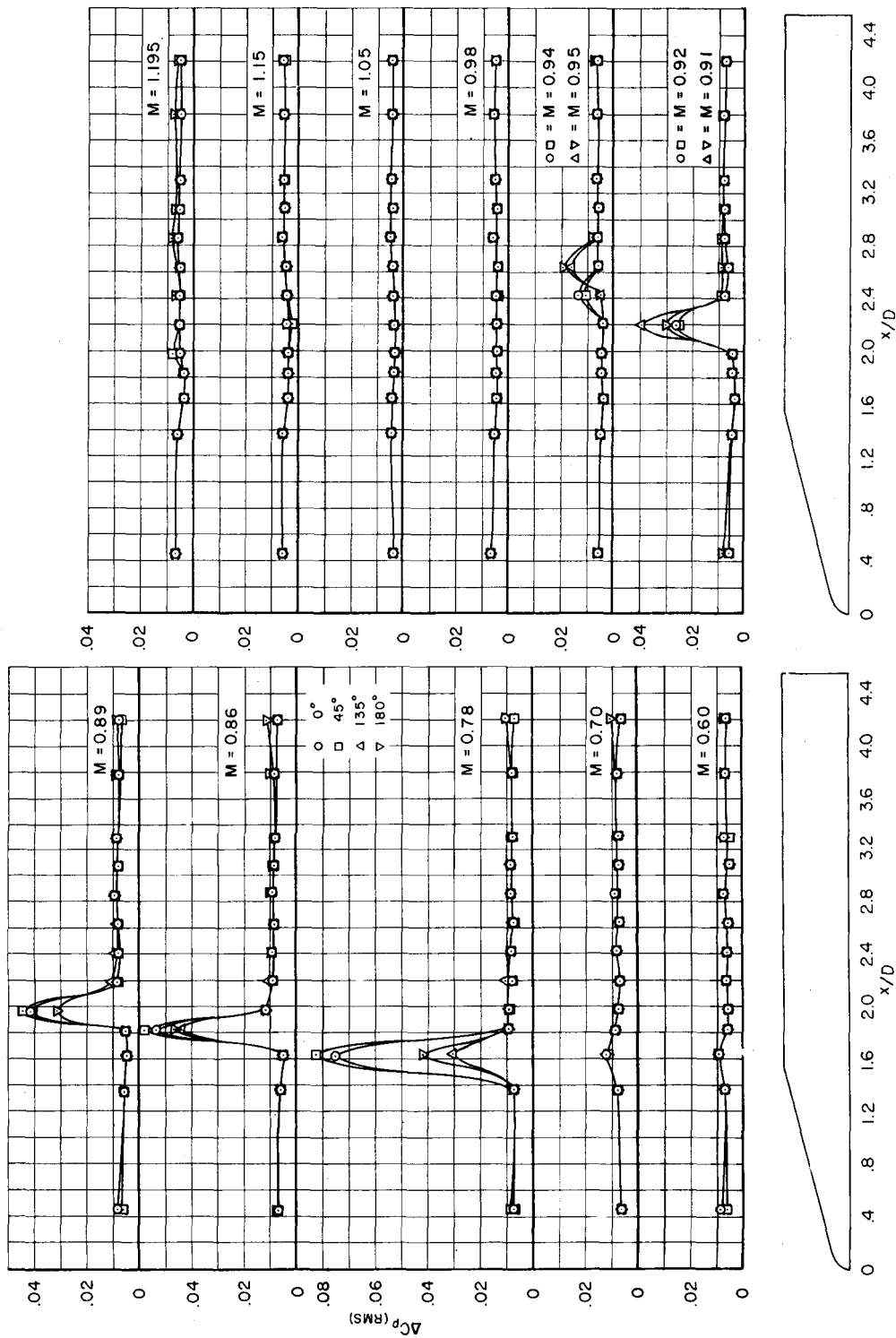
(a)  $\alpha = 0^\circ$

Figure 7.- Longitudinal distributions of the pressure fluctuations on the Centaur model.

DECLASSIFIED

CONFIDENTIAL

21

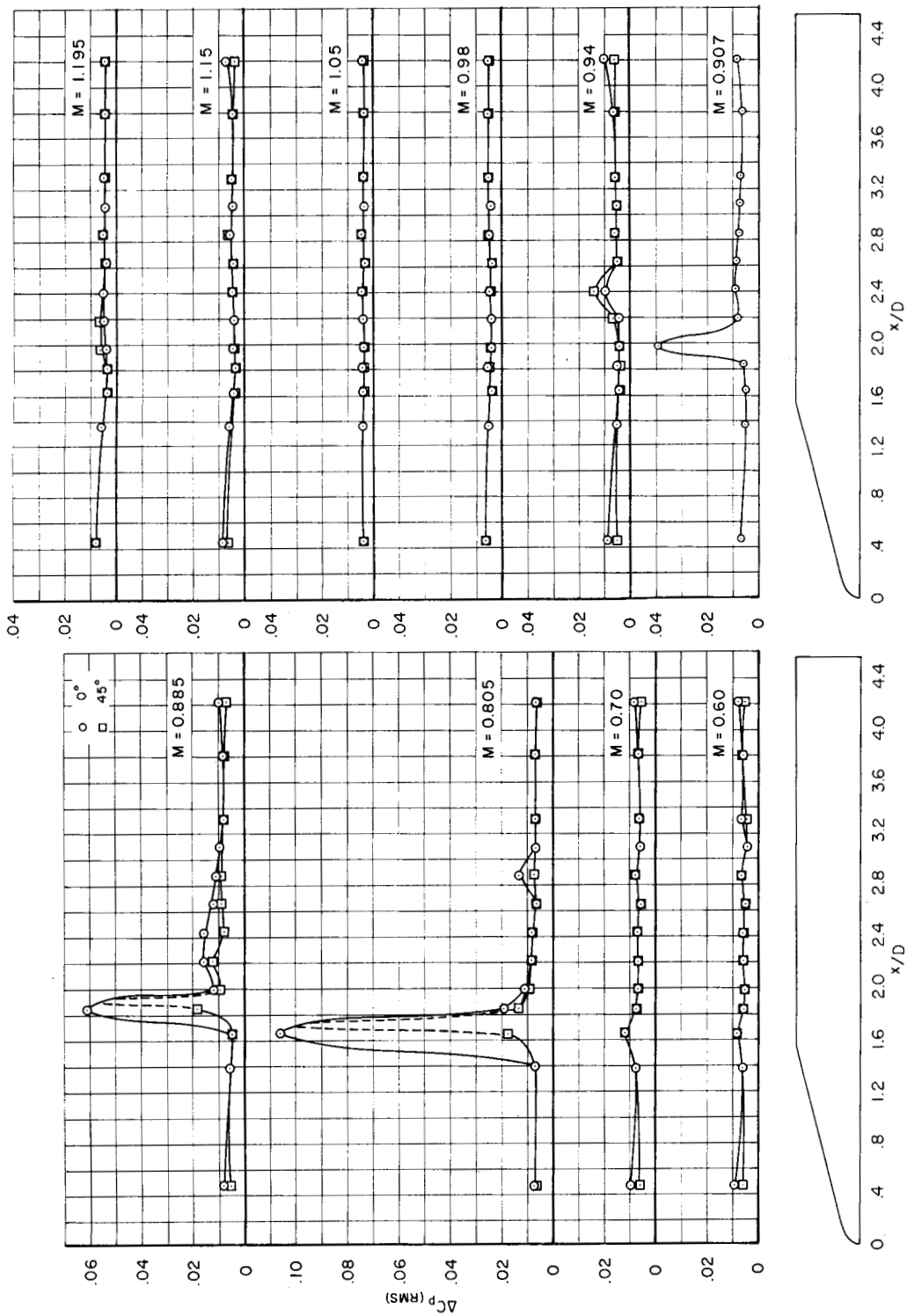


(b)  $\alpha = 4^\circ$

Figure 7.- Continued.

A  
4  
6  
5

CONFIDENTIAL



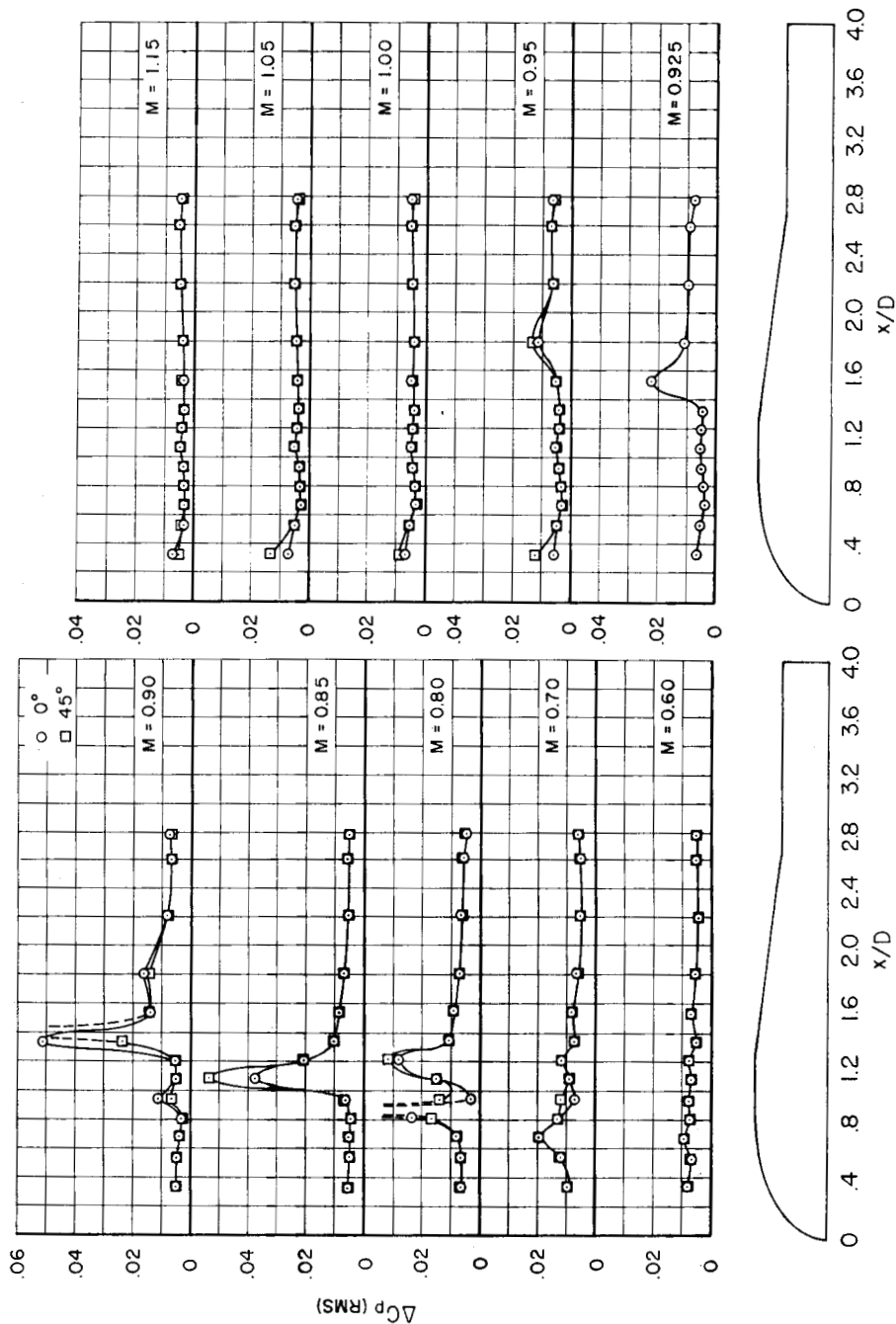
(c)  $\alpha = 8^\circ$

Figure 7.- Concluded.

REF ID: A665

CONFIDENTIAL

23

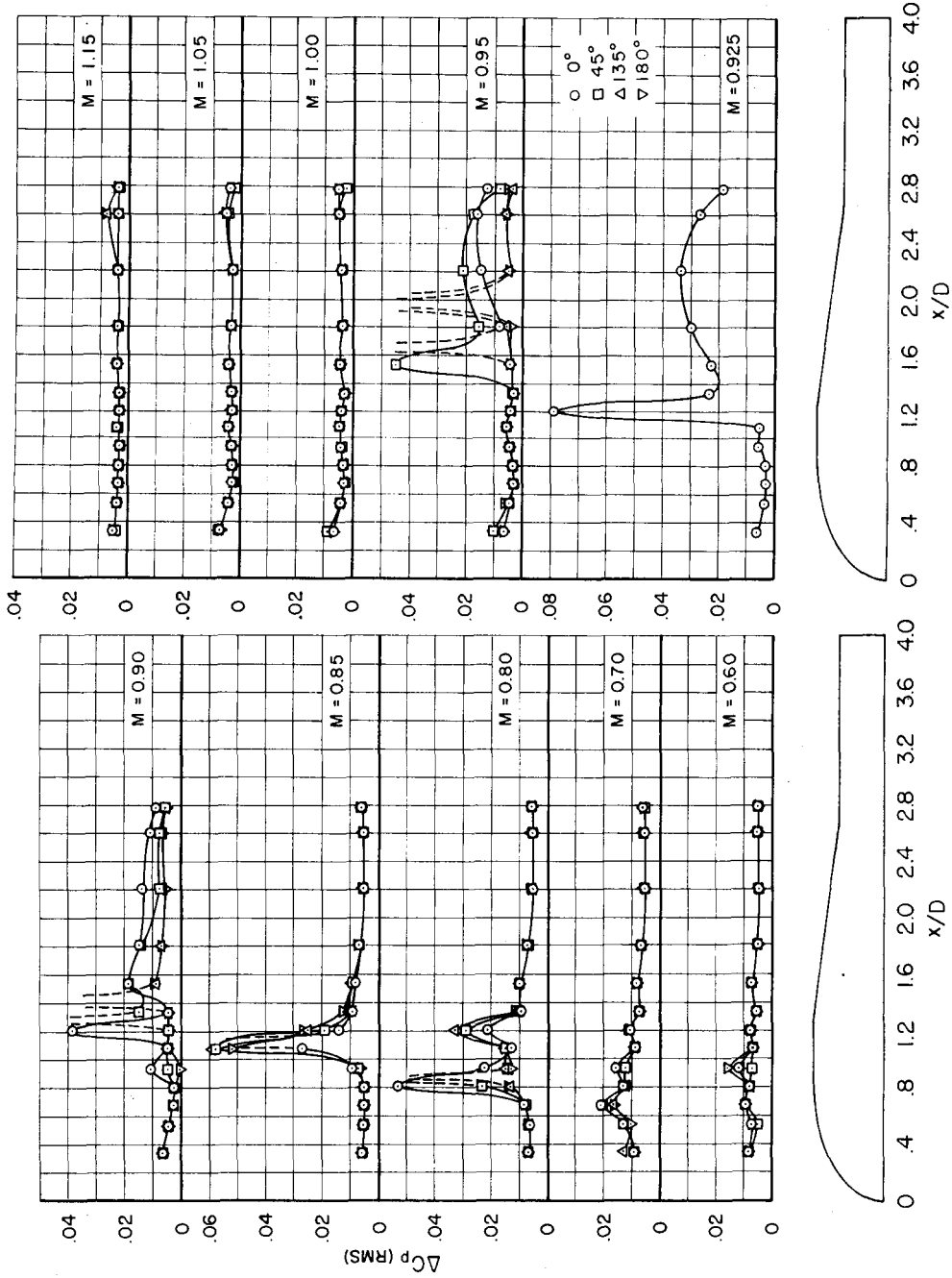


(a)  $\alpha = 0^\circ$

Figure 8.-- Longitudinal distributions of the pressure fluctuations on the Able-V model.



03 9030 030



(b)  $\alpha = 3^\circ$   
Figure 8.- Continued.

# DECLASSIFIED

CONFIDENTIAL

25

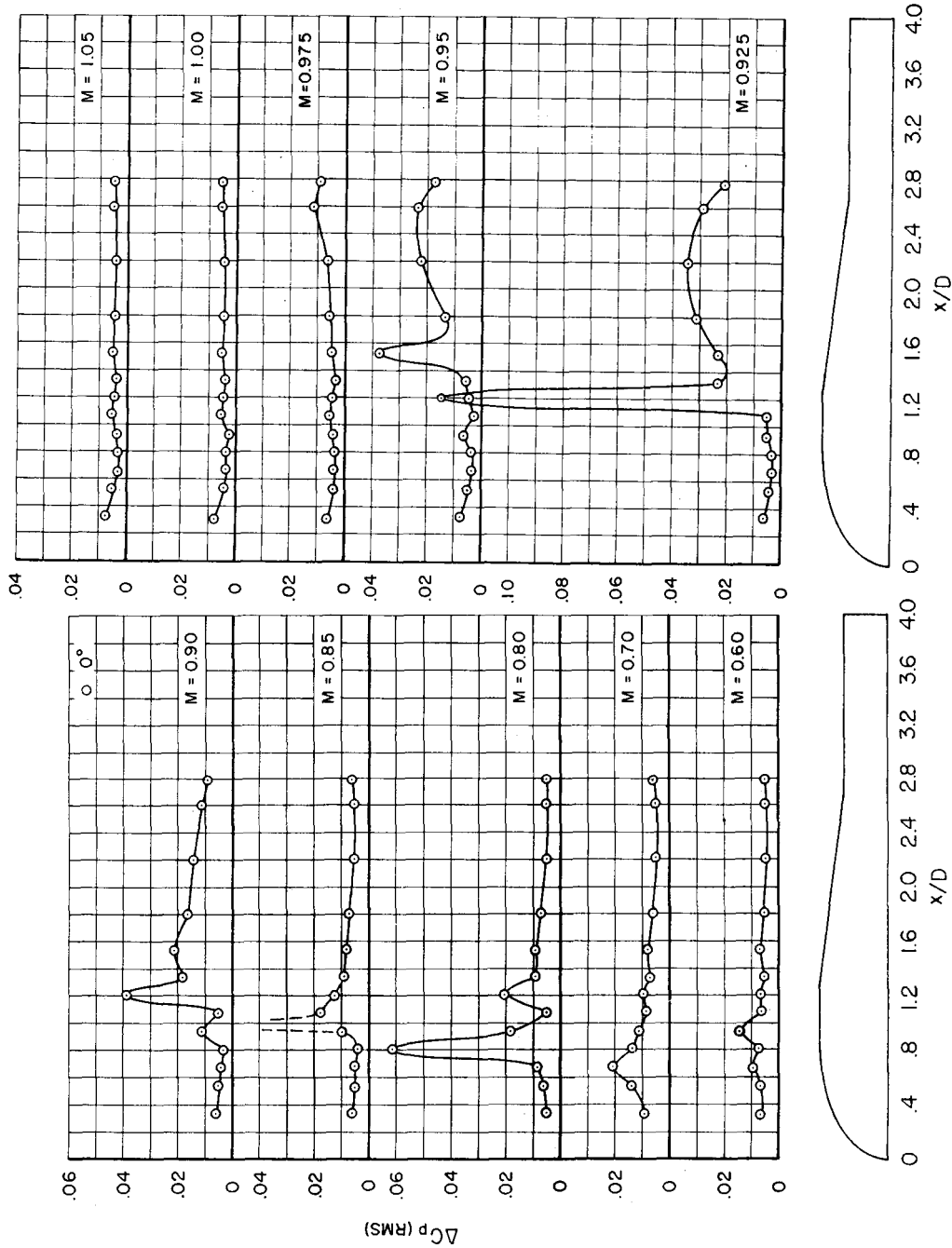
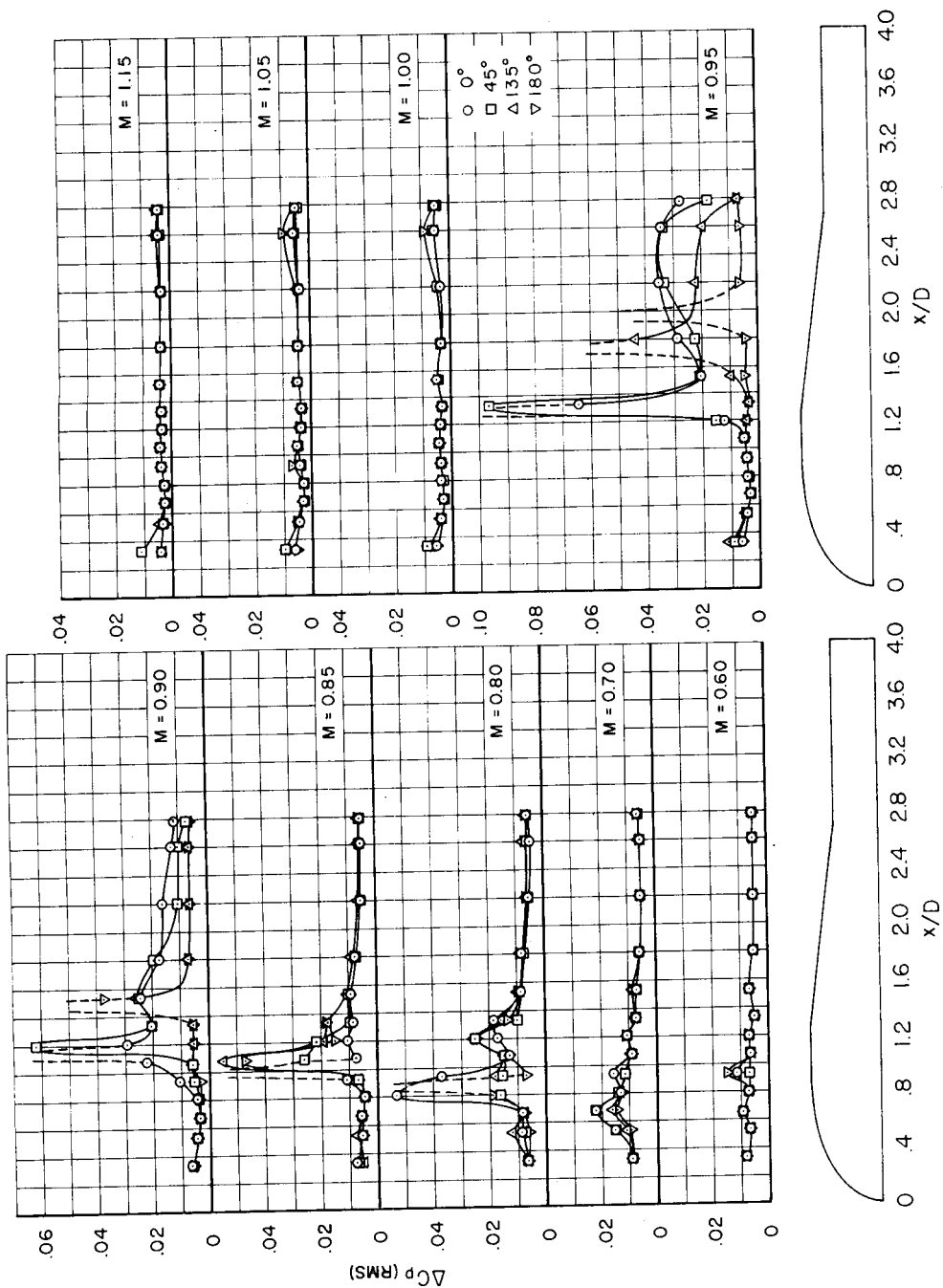


Figure 8.- Continued.

(c)  $\alpha = 4^\circ$



(d)  $\alpha = 6^\circ$

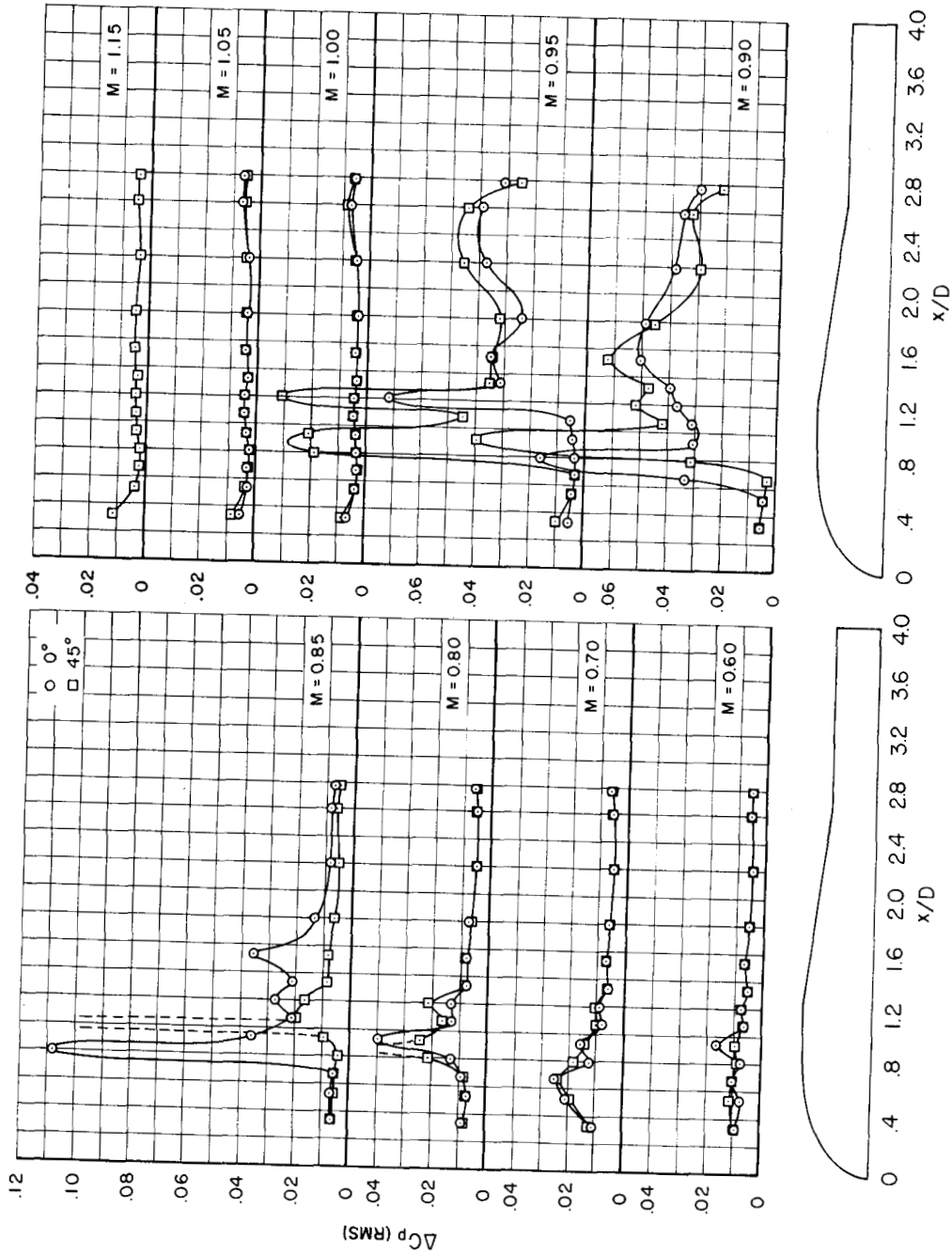
Figure 8.- Continued.

# DECLASSIFIED

CONFIDENTIAL

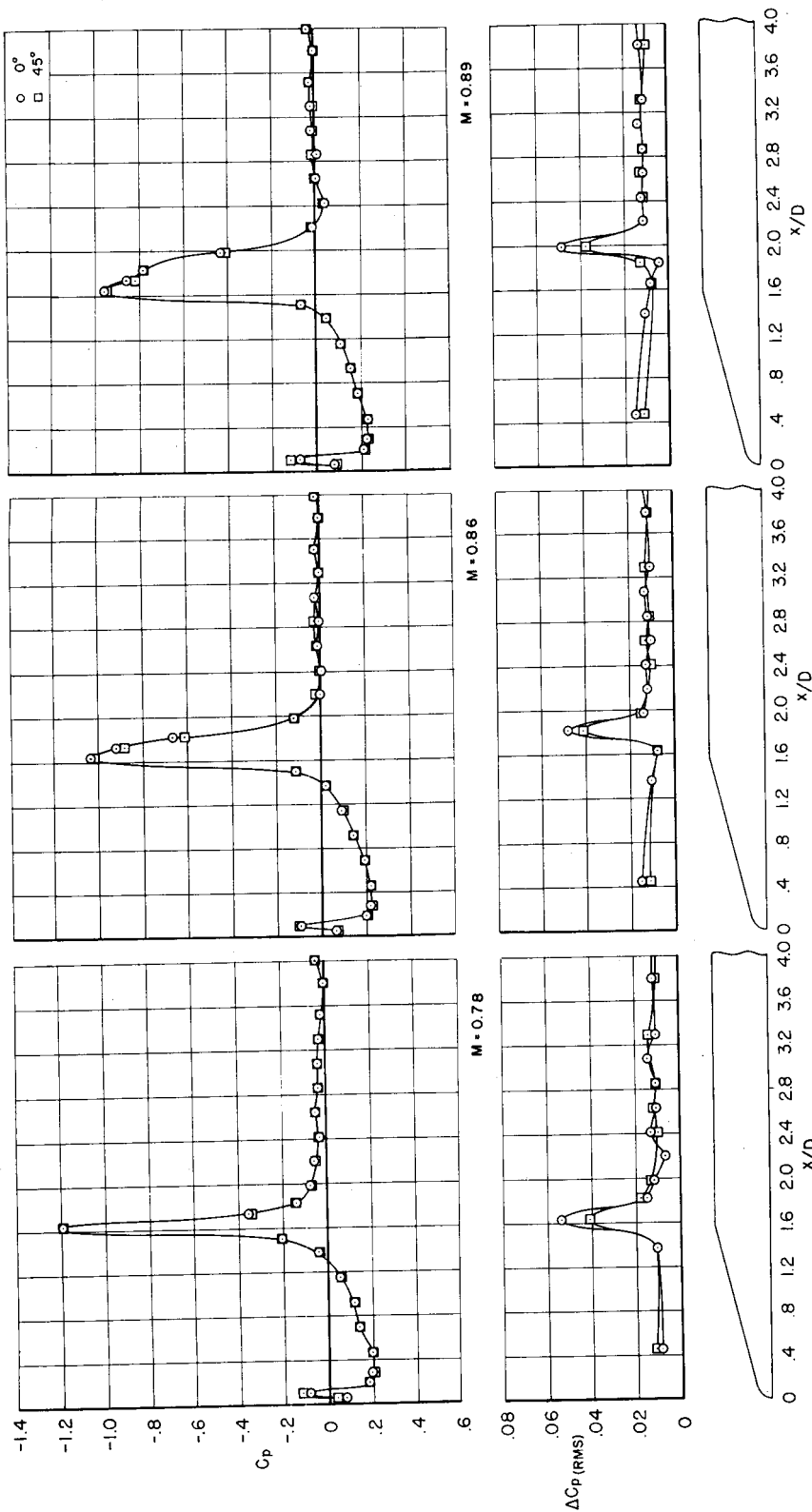
27

A  
4  
6  
5



(e)  $\alpha = 10^\circ$

Figure 8.- Concluded.



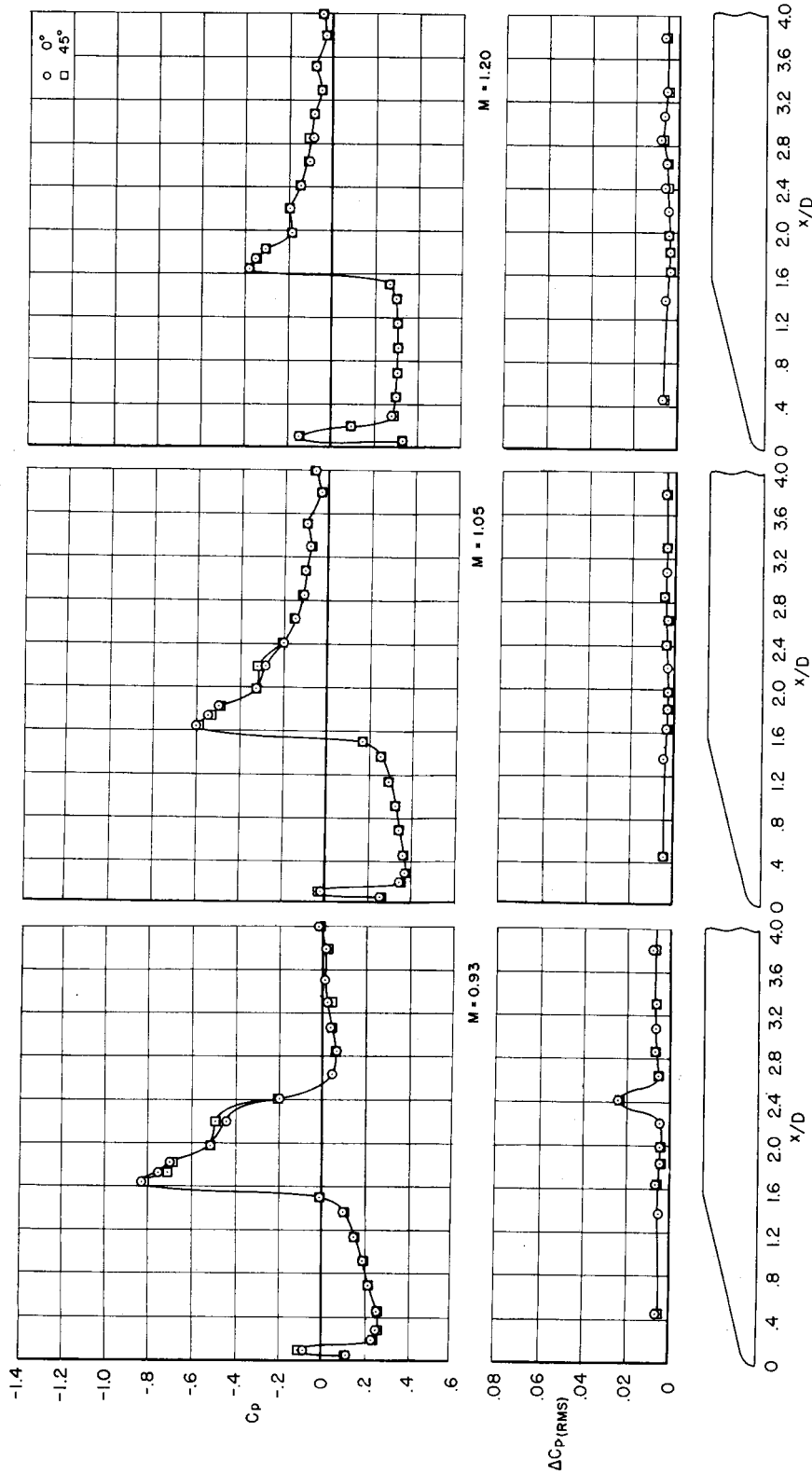
(a)  $\alpha = 0^\circ$

Figure 9.- Pressure fluctuations and time-average static-pressure distributions on the Centaur model.

DECLASSIFIED

CONFIDENTIAL

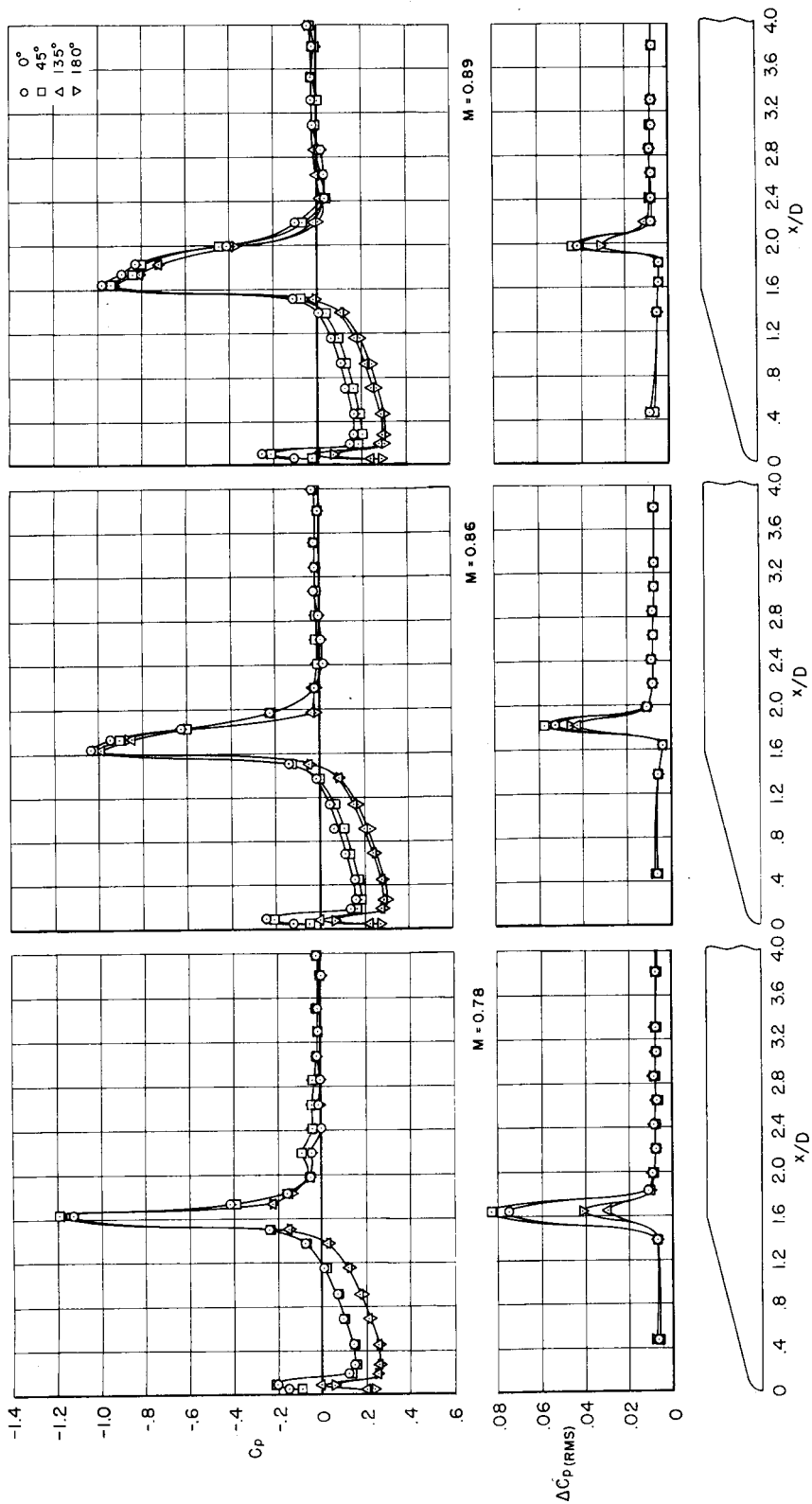
29



(a)  $\alpha = 0^\circ$  - Concluded.

Figure 9.- Continued.

A  
4  
6  
5

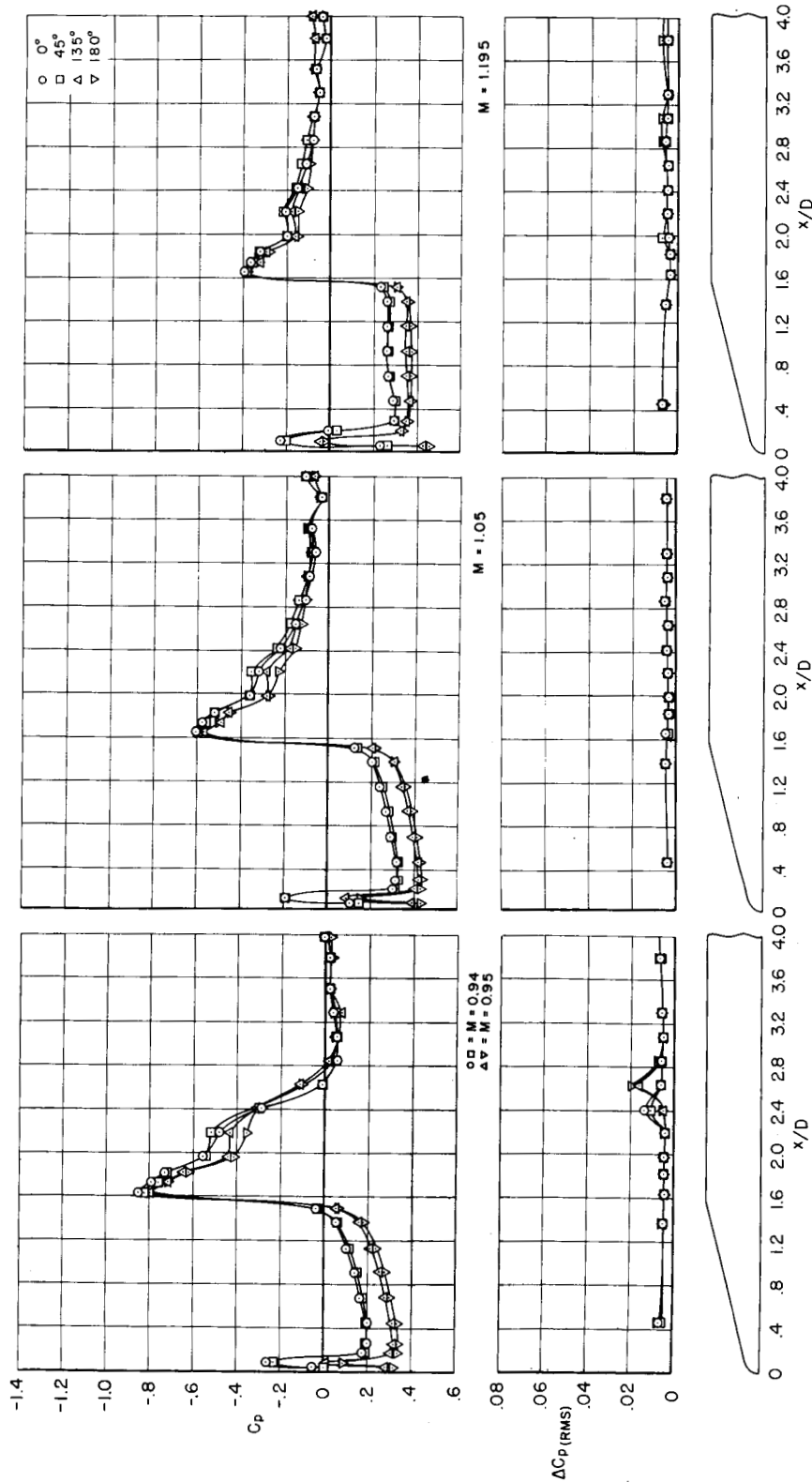


(b)  $\alpha = 40^\circ$   
Figure 9.- Continued.

CONFIDENTIAL

CONFIDENTIAL

31

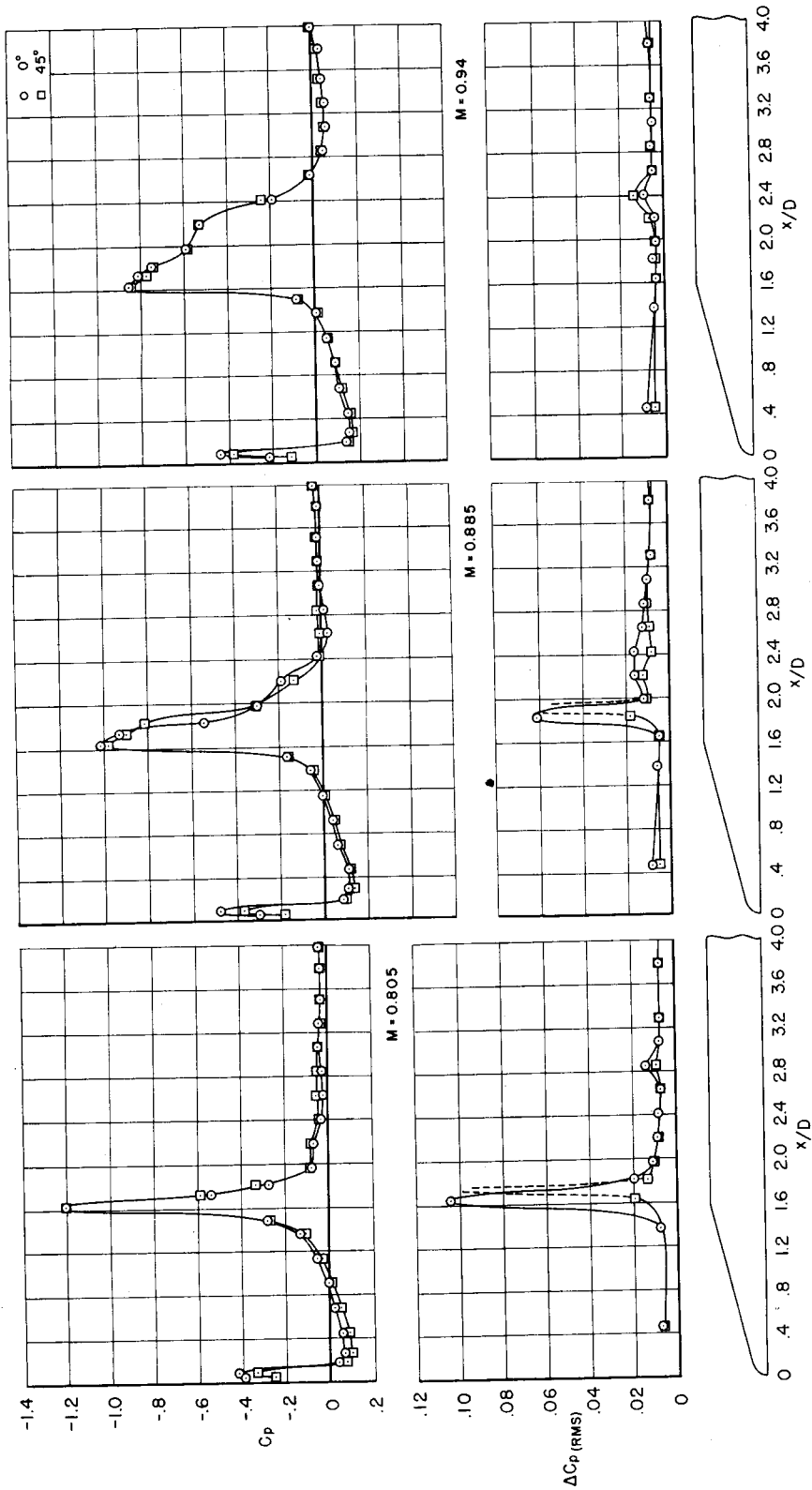


(b)  $\alpha = 4^\circ$  - Concluded.

Figure 9.- Continued.



CONFIDENTIAL

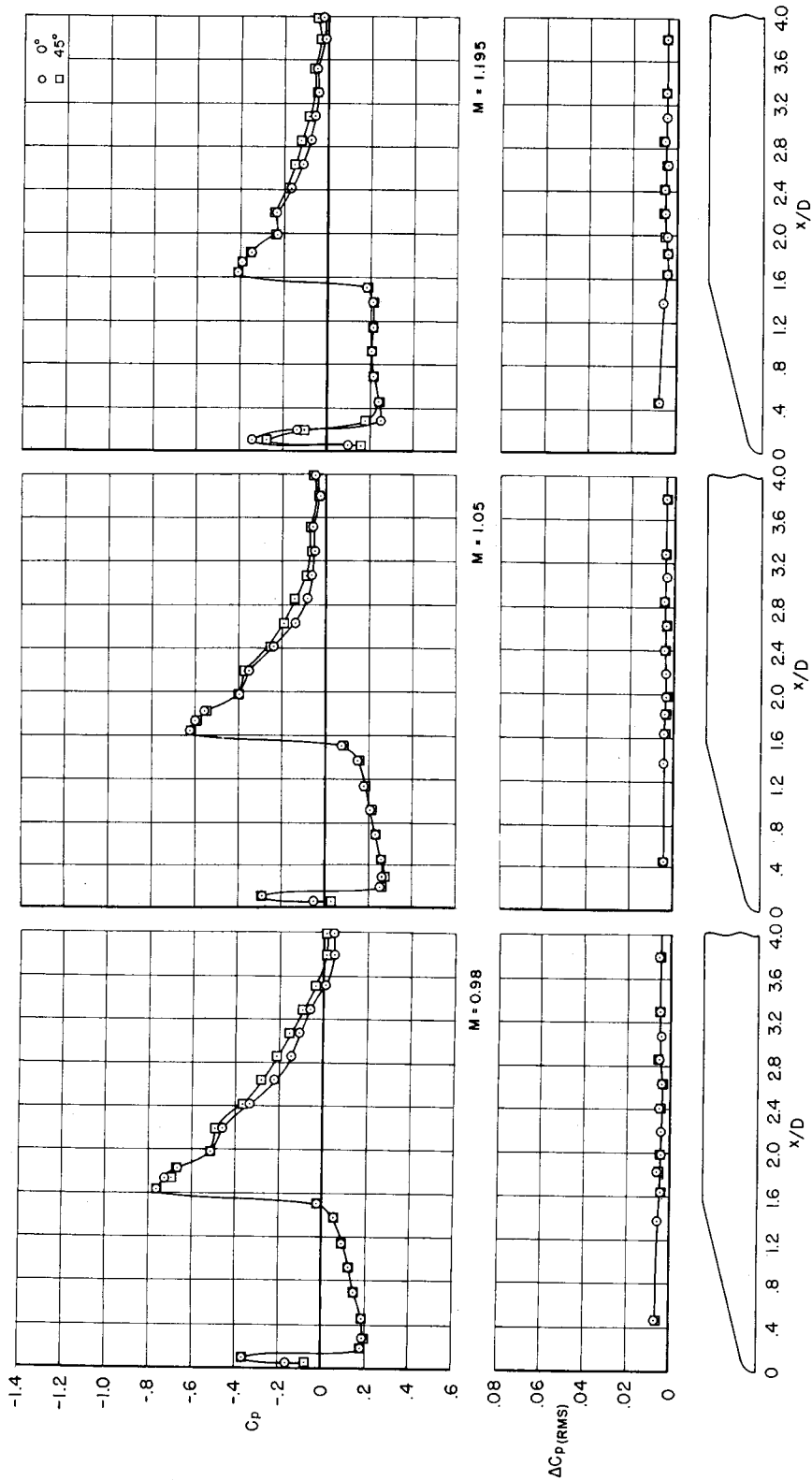


(c)  $\alpha = 8^\circ$

Figure 9.- Continued.

DECLASSIFIED

CONFIDENTIAL



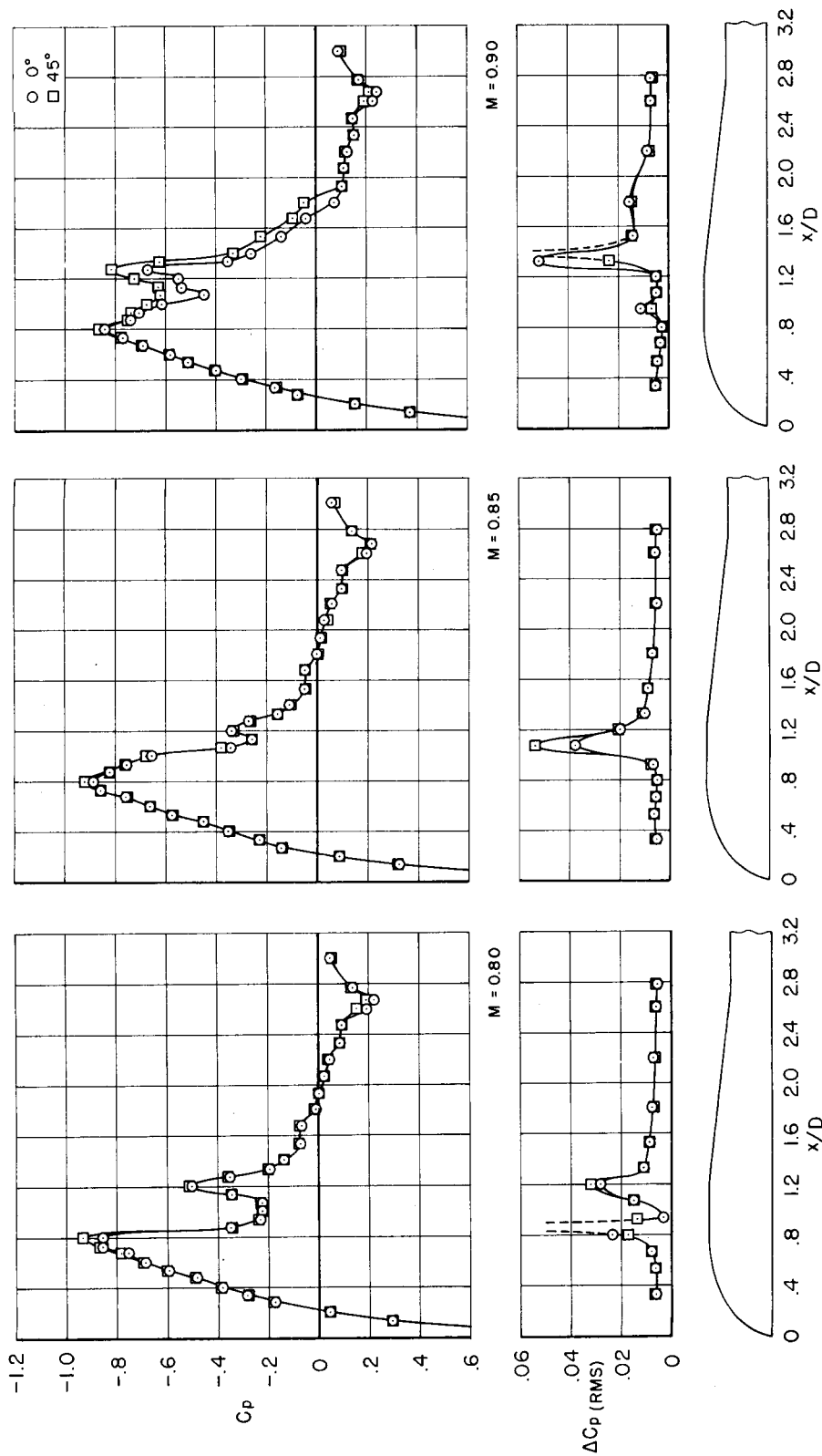
(c)  $\alpha = 8^\circ$  - Concluded.

Figure 9.- Concluded.

CONFIDENTIAL

34

CONFIDENTIAL



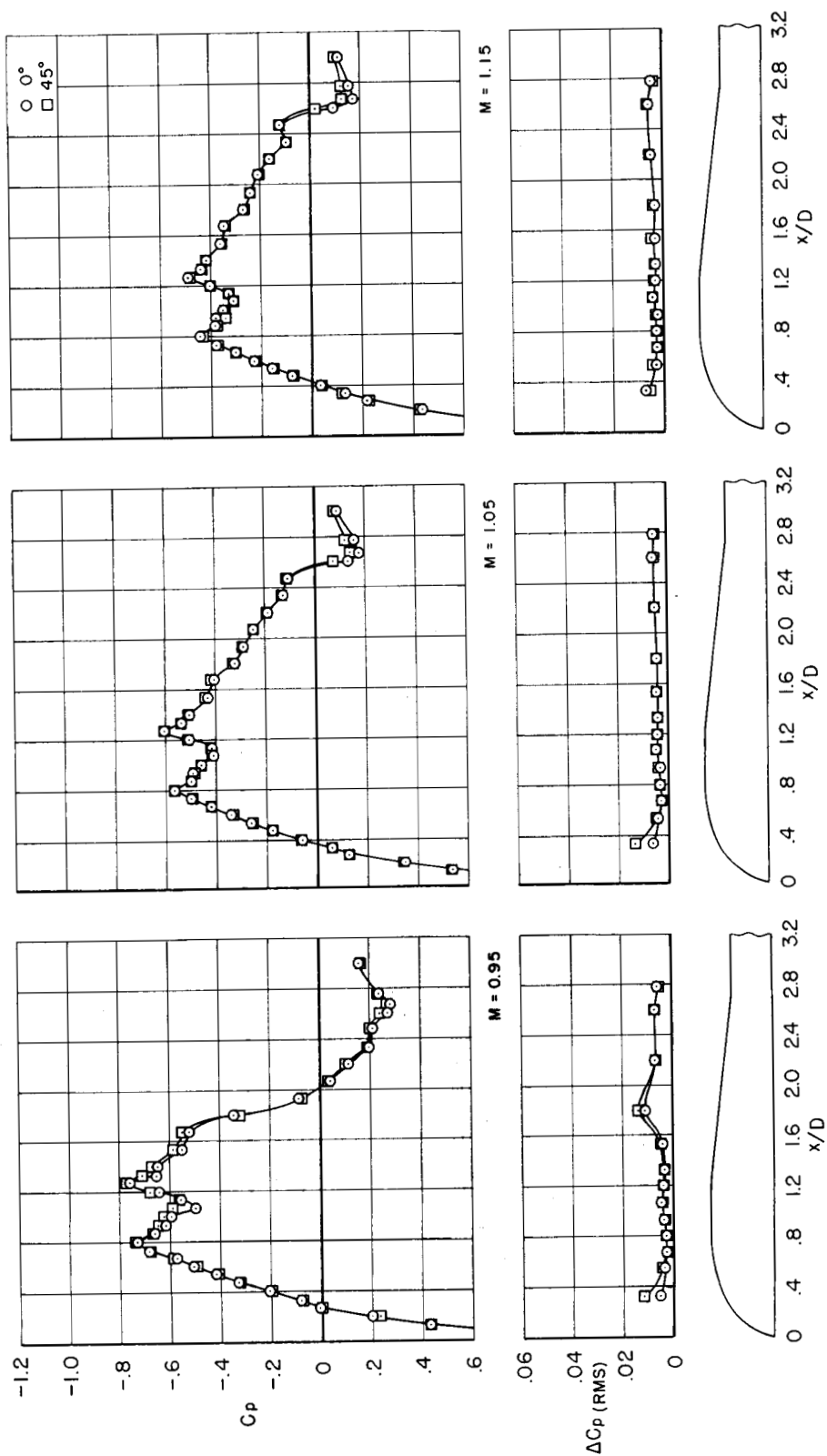
(a)  $\alpha = 0^\circ$   
model.

Figure 10.- Pressure fluctuations and time-average static-pressure distributions on the Able-V model.

DECLASSIFIED

CONFIDENTIAL

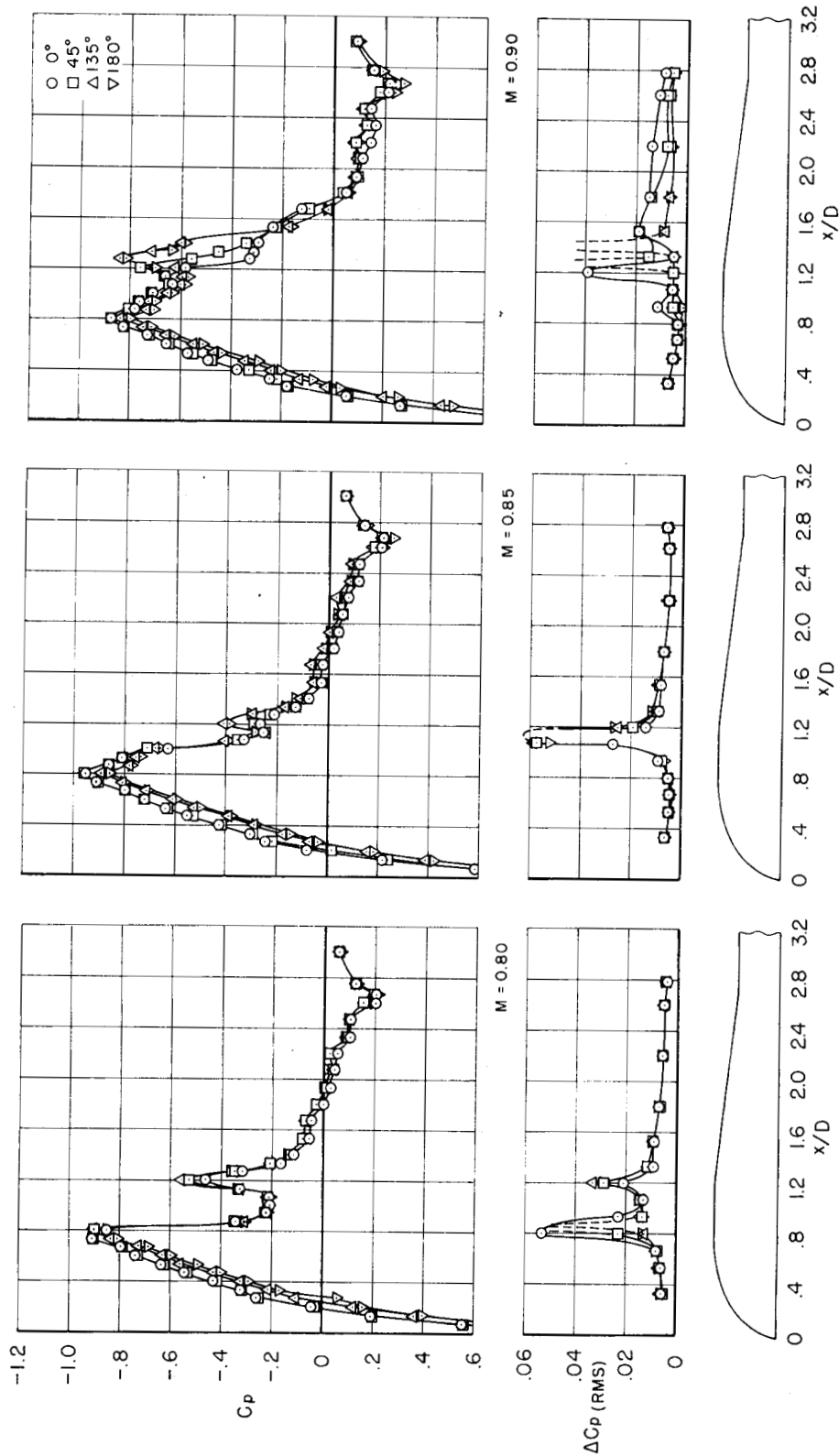
35



(a)  $\alpha = 0^\circ$  - Concluded.

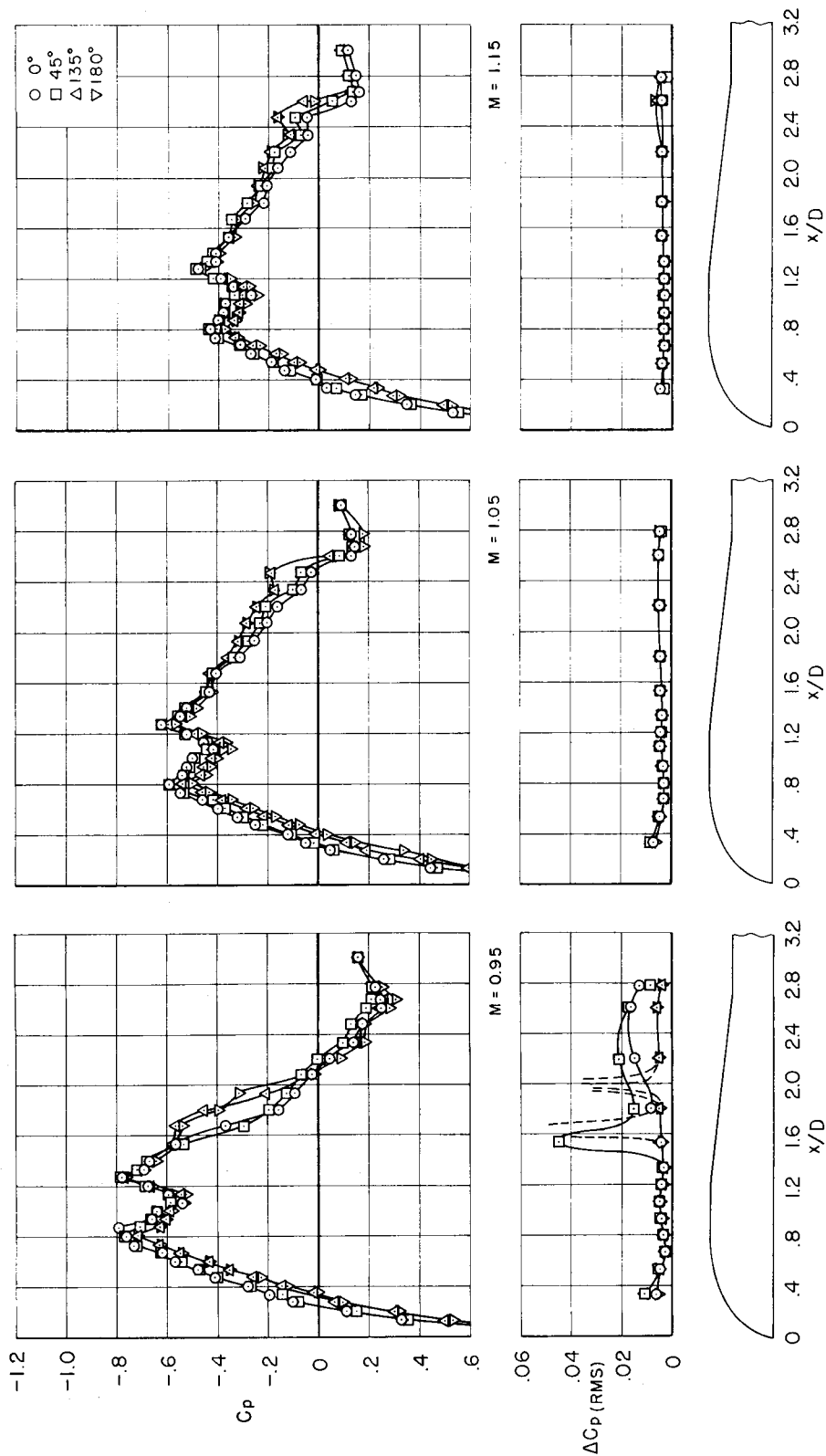
Figure 10.- Continued.

A  
4  
6  
5



(b)  $\alpha = 3^\circ$

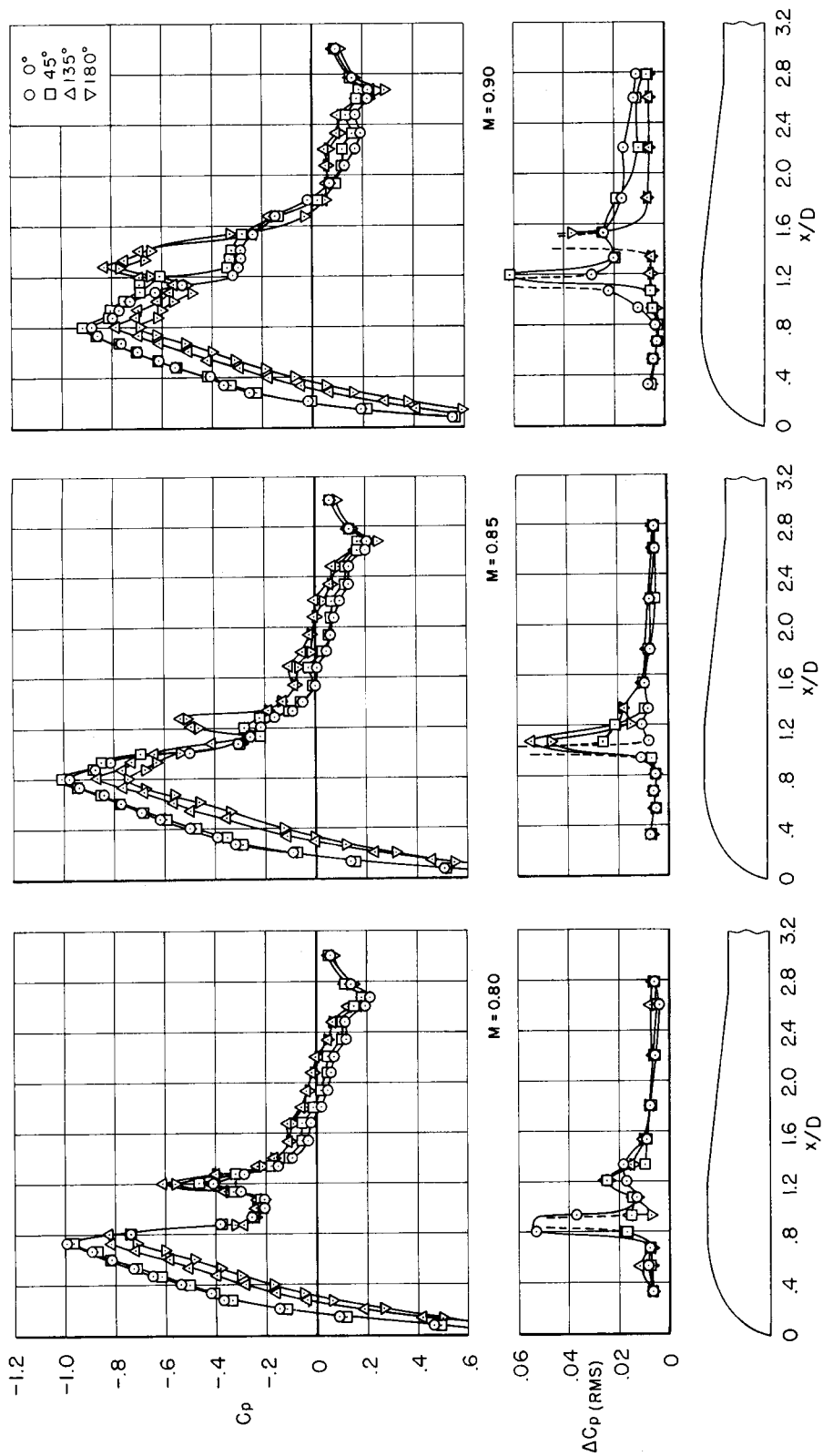
Figure 10.- Continued.



(b)  $\alpha = 3^\circ$  - Concluded.

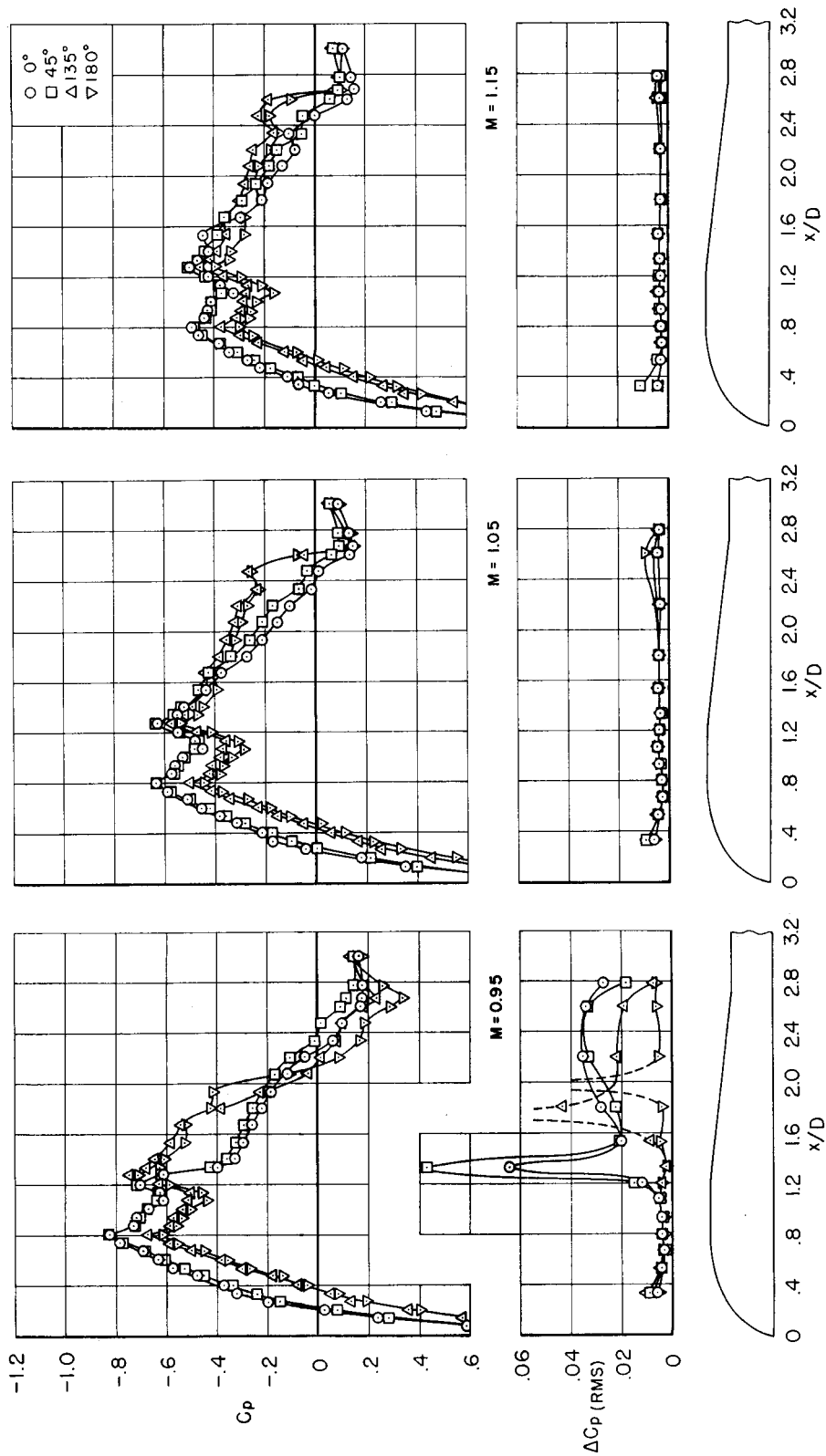
Figure 10.- Continued.

CONFIDENTIAL



(c)  $\alpha = 6^\circ$

Figure 10.- Continued.

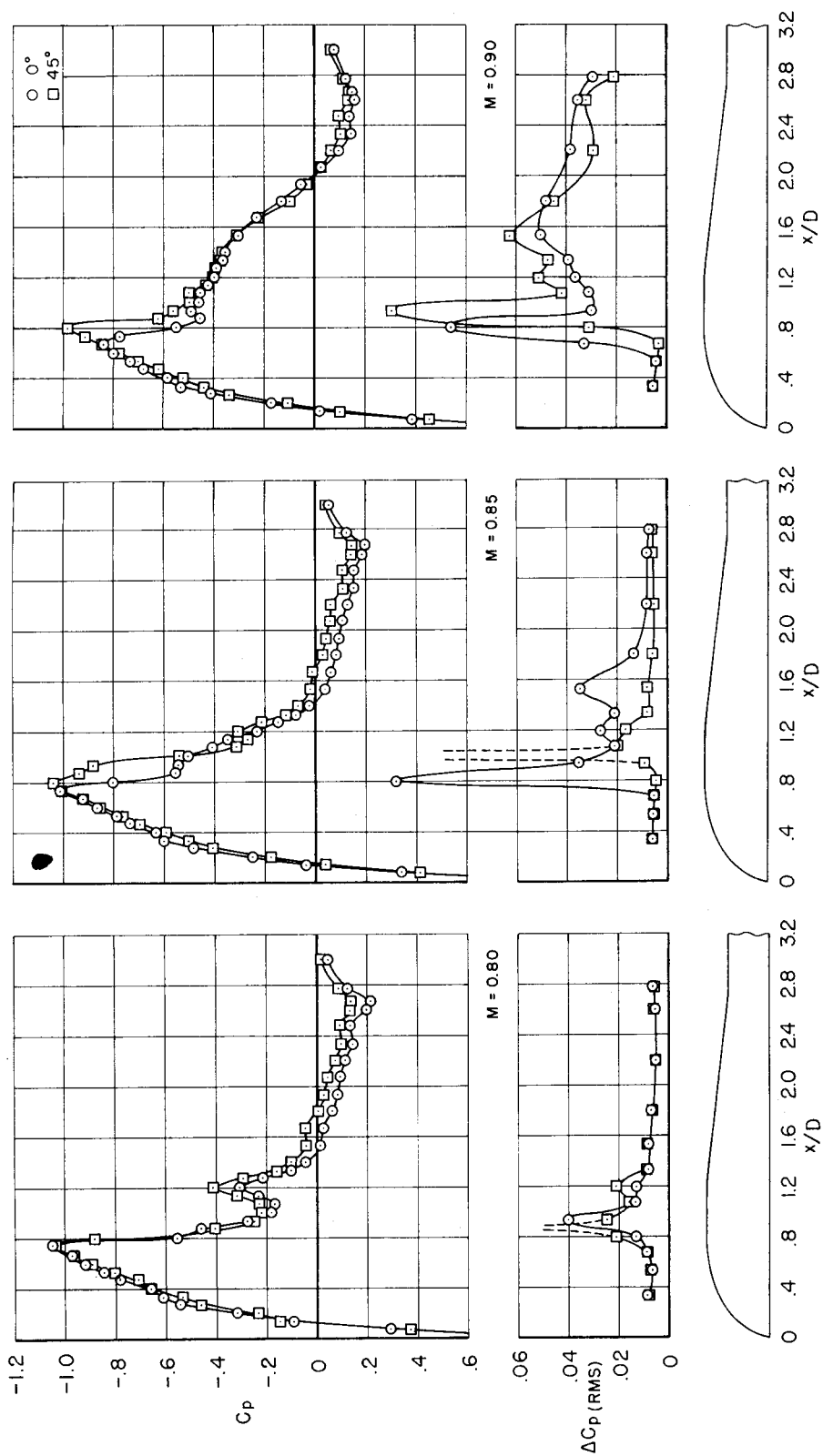


(c)  $\alpha = 6^\circ$  - Concluded.

Figure 10.- Continued.

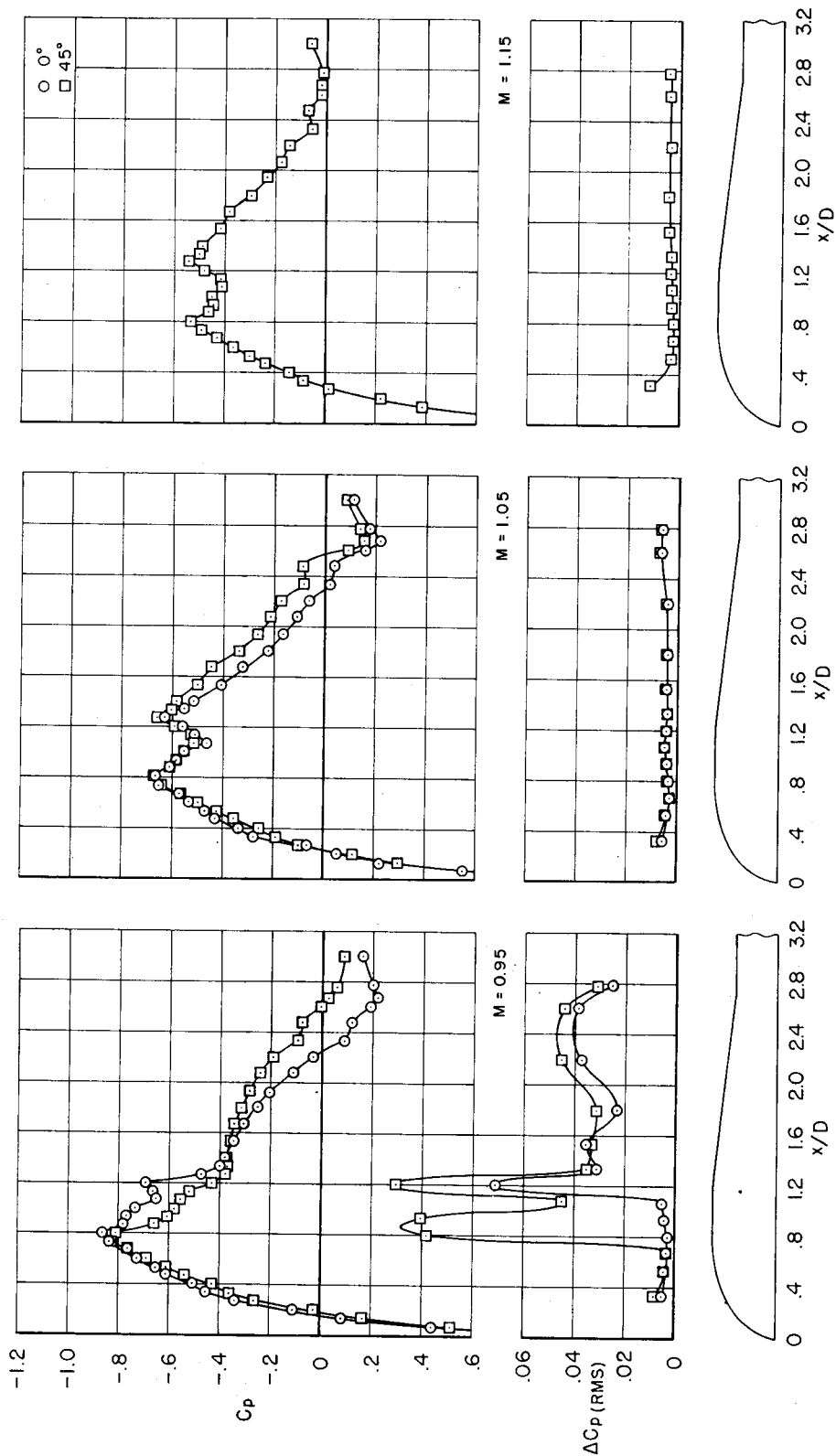


CONFIDENTIAL



(d)  $\alpha = 10^\circ$

Figure 10.- Continued.



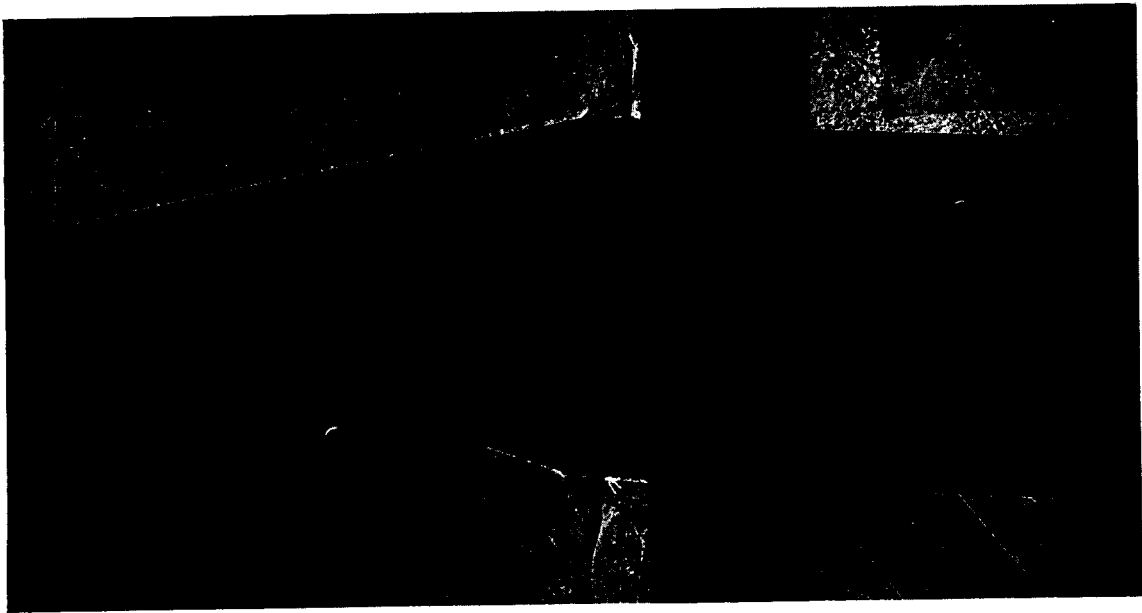
(d)  $\alpha = 10^\circ$  - Concluded.

Figure 10.- Concluded.

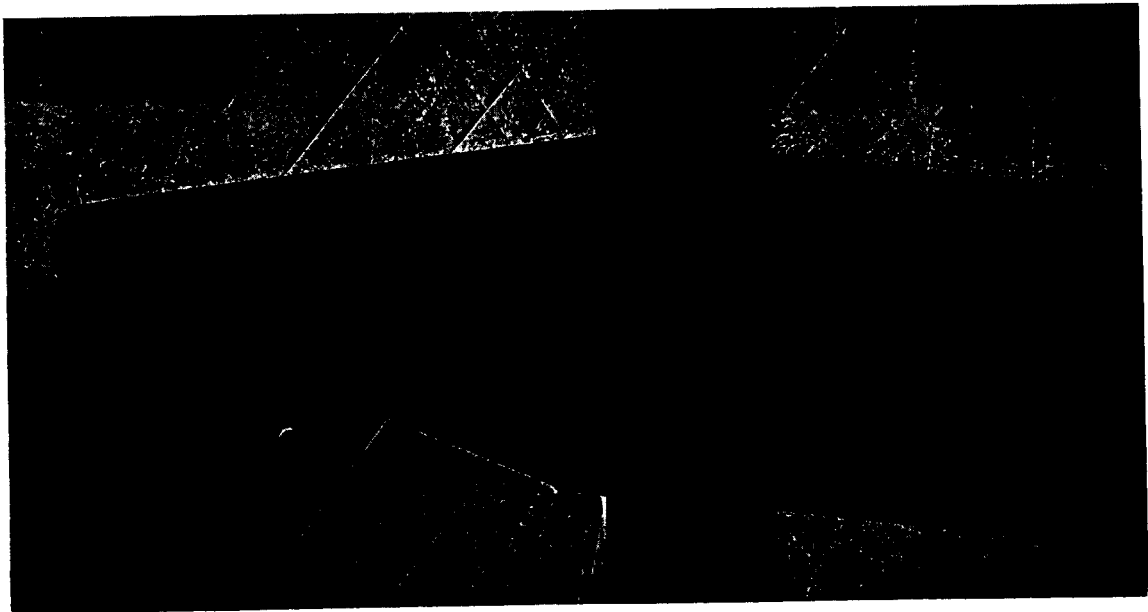
03712201030

42

CONFIDENTIAL



$$M = 0.78, \alpha = 4^\circ$$



$$M = 0.805, \alpha = 8^\circ$$

(a) Centaur model.

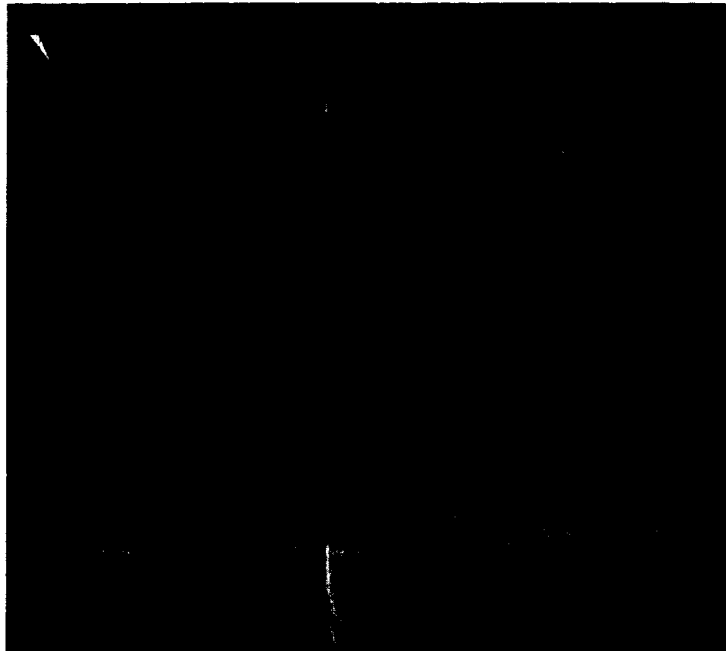
Figure 11.- Typical shadowgraph pictures of the flow when large pressure fluctuations were occurring.

A  
4  
6  
5

DECLASSIFIED

CONFIDENTIAL

43



$$M = 0.90, \alpha = 3^\circ$$



$$M = 0.95, \alpha = 6^\circ$$

(b) Able-V model.

Figure 11.- Concluded.



A  
4  
6  
5

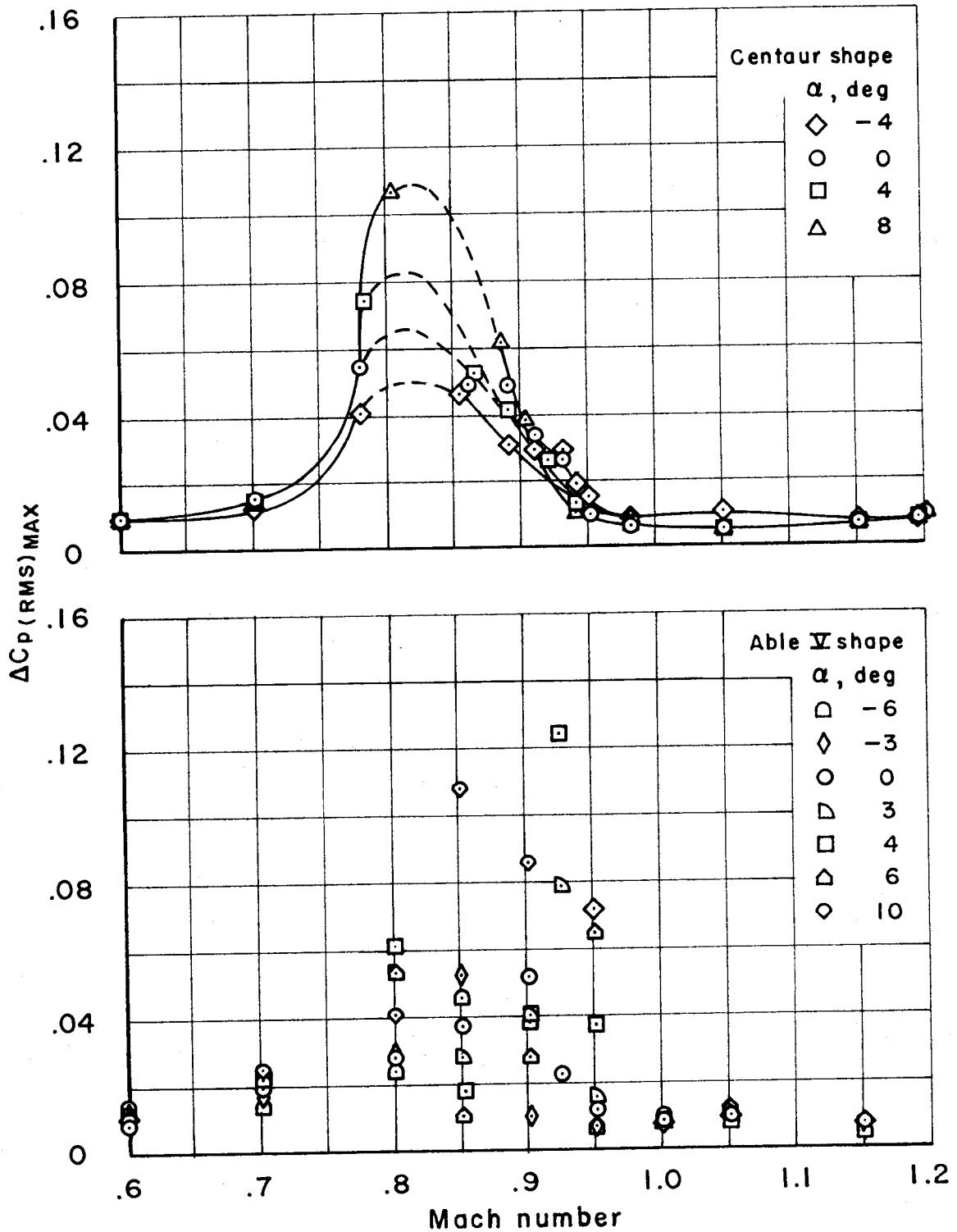
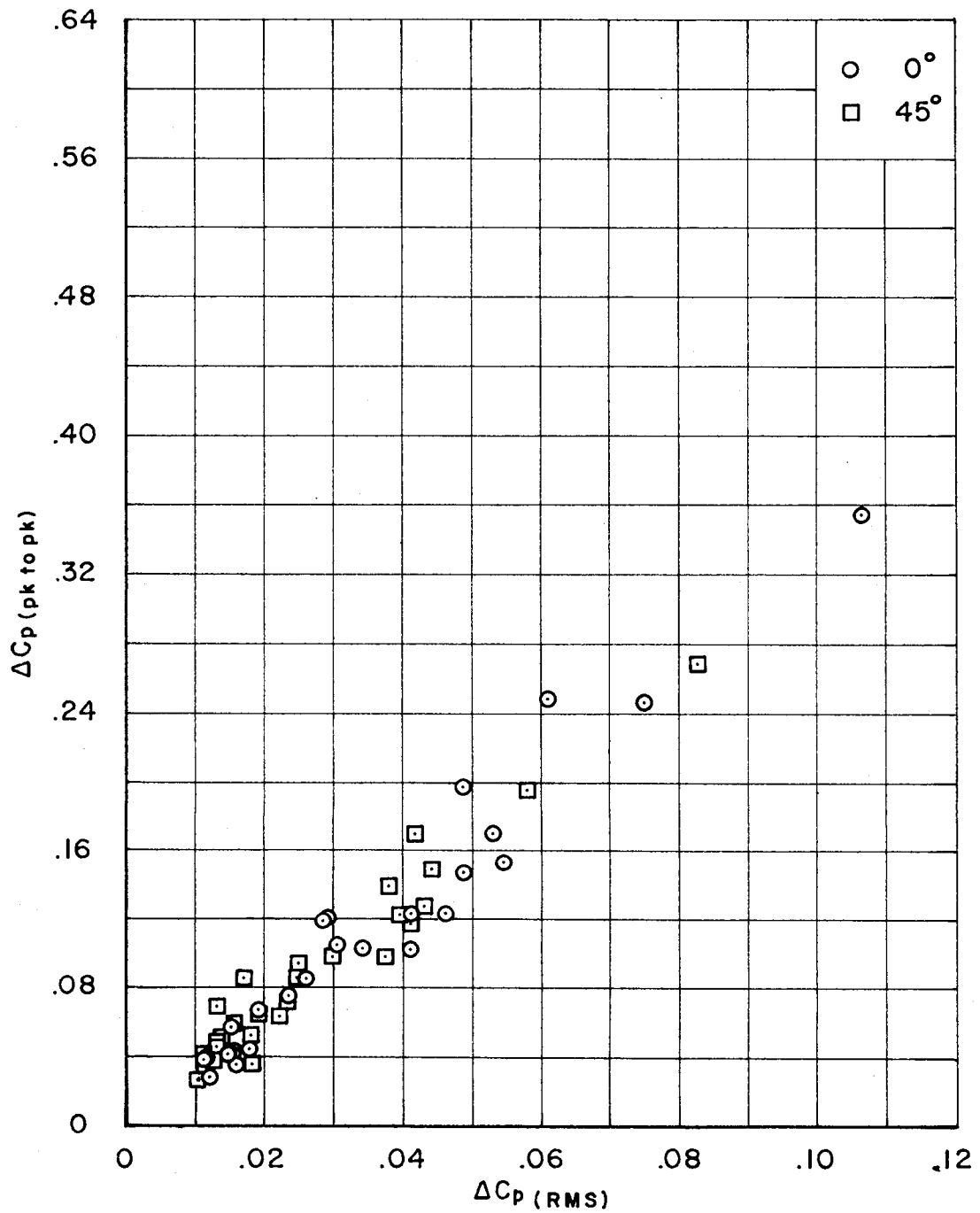


Figure 12.- The variation with Mach number of the maximum pressure fluctuations measured along the top centerline of the models.

DECLASSIFIED

CONFIDENTIAL

45



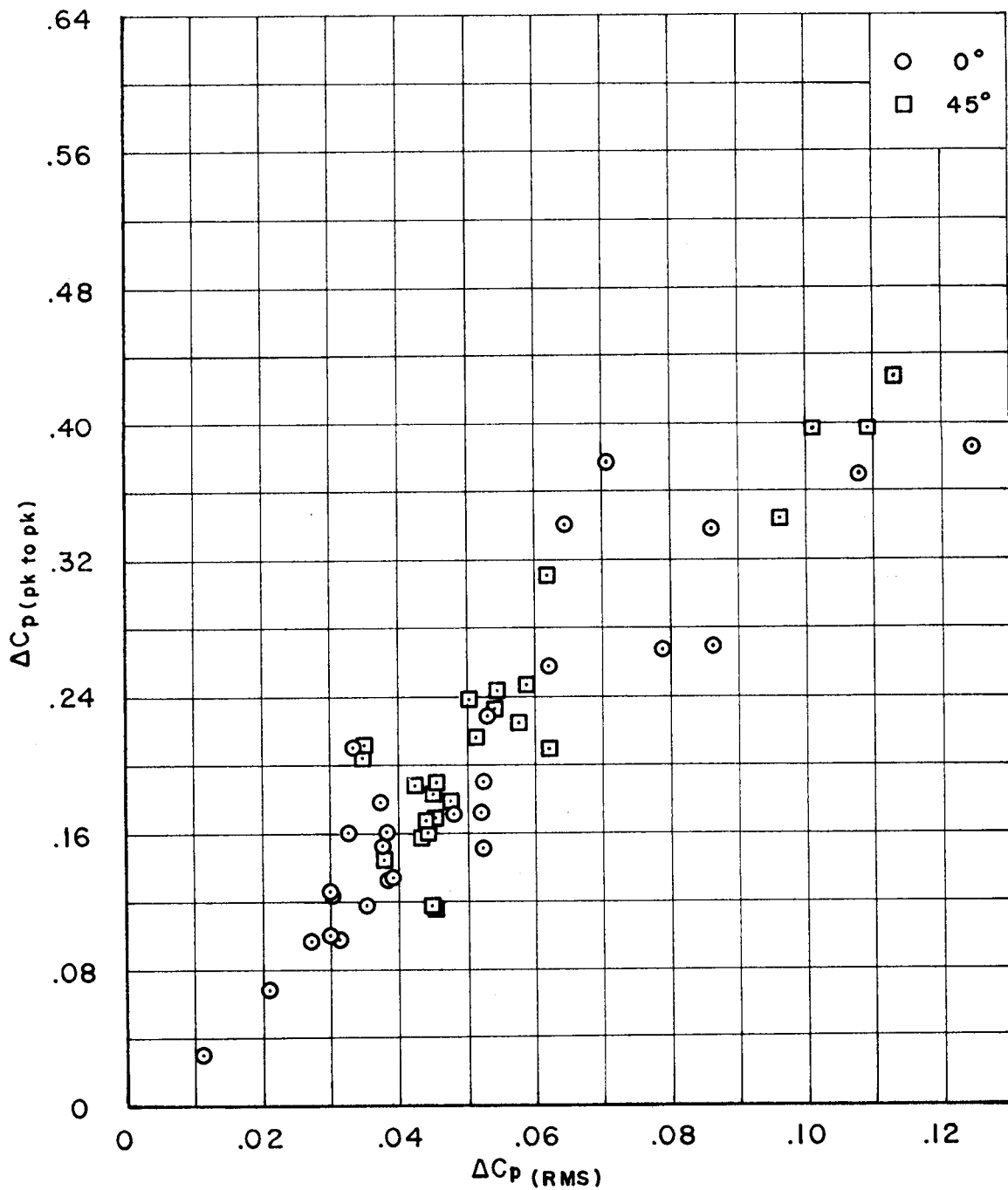
(a) Centaur model.

Figure 13.- The relationship between peak-to-peak and RMS measurements of the pressure-fluctuation intensity.

037122A.1030

46

CONFIDENTIAL



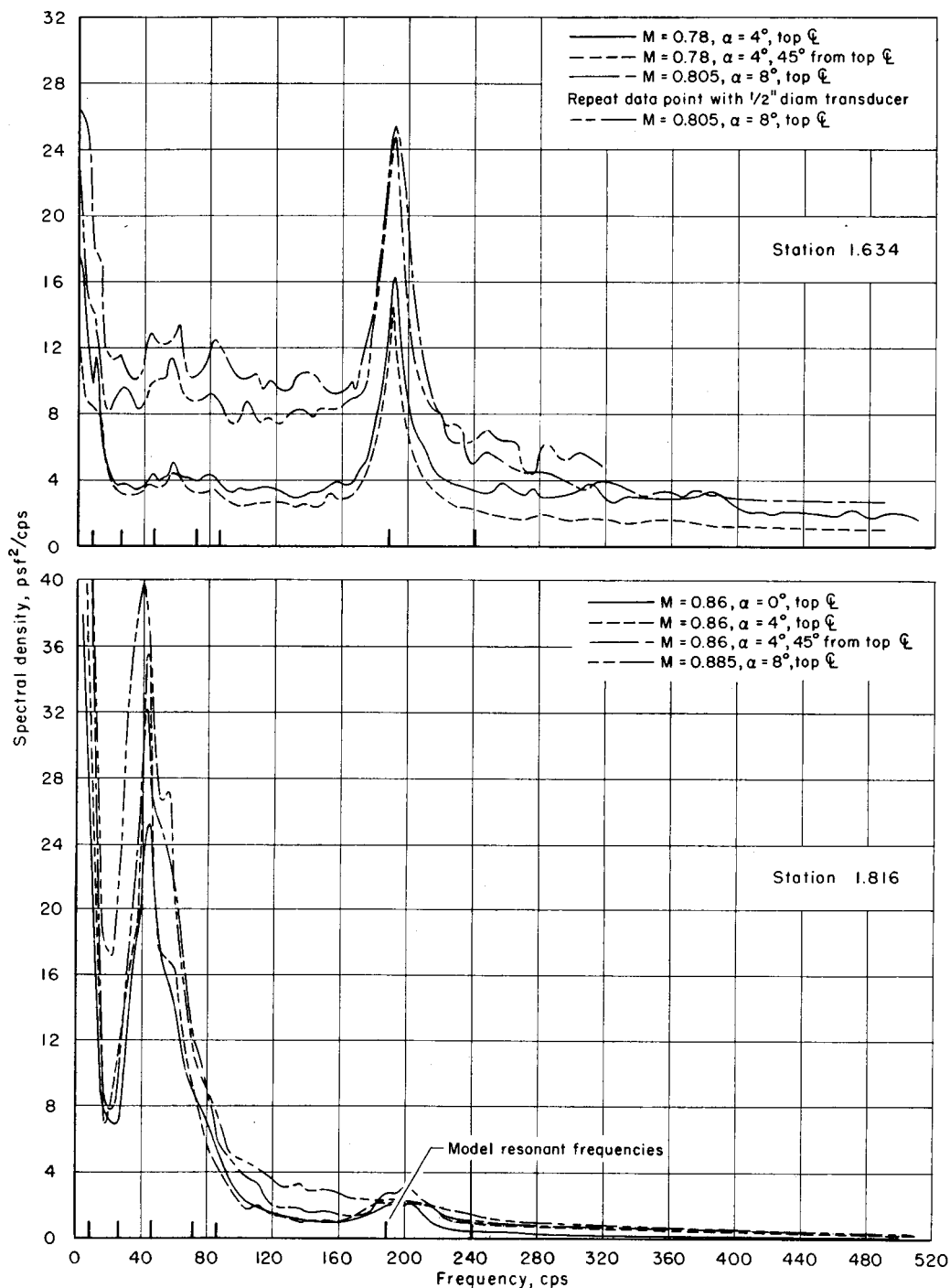
(b) Able-V model.

Figure 13.- Concluded.

DECLASSIFIED

CONFIDENTIAL

47



(a) Centaur model.

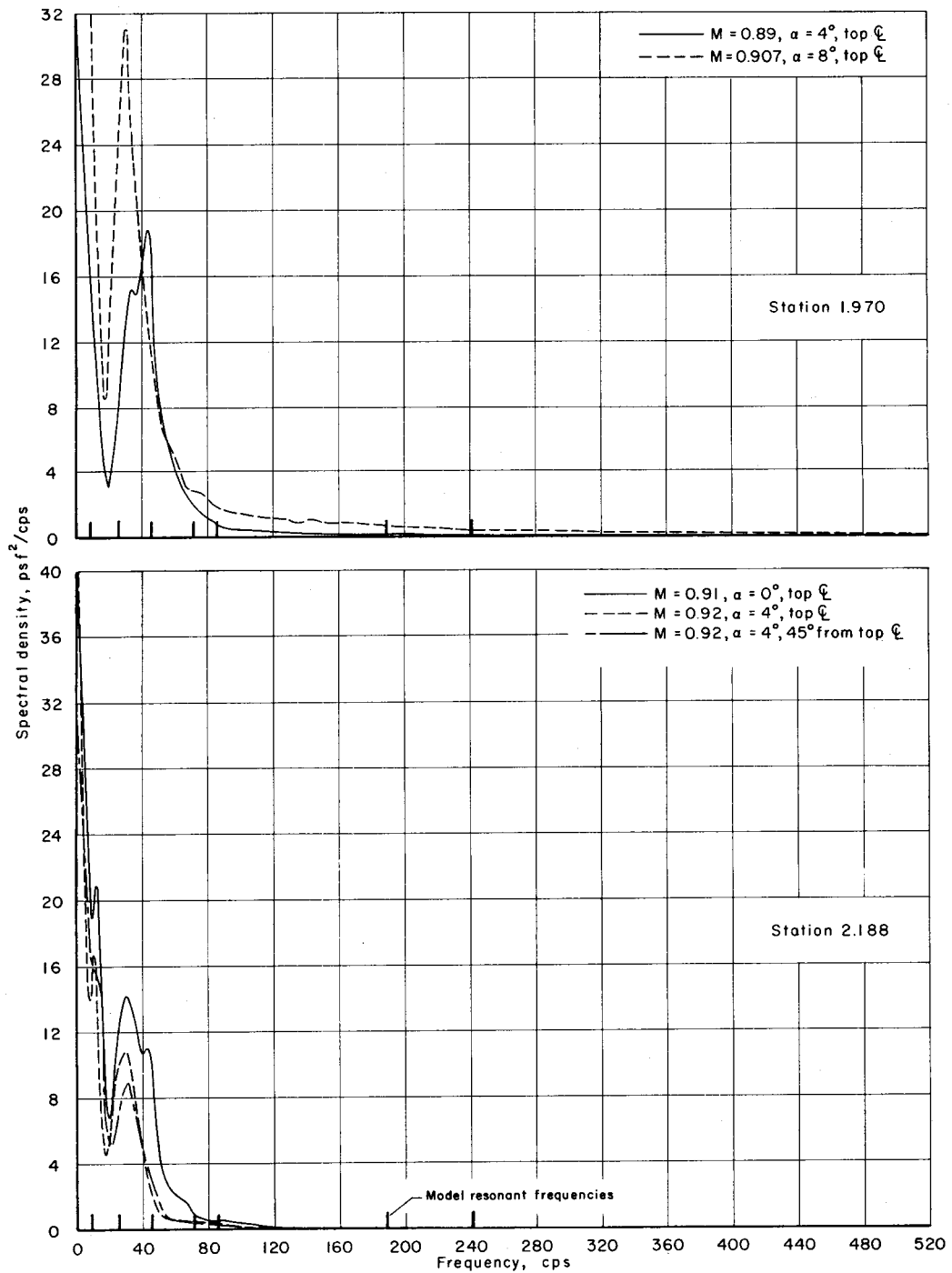
Figure 14.- Power spectral densities of pressure fluctuations at the normal shock wave.



03752A1030

48

CONFIDENTIAL



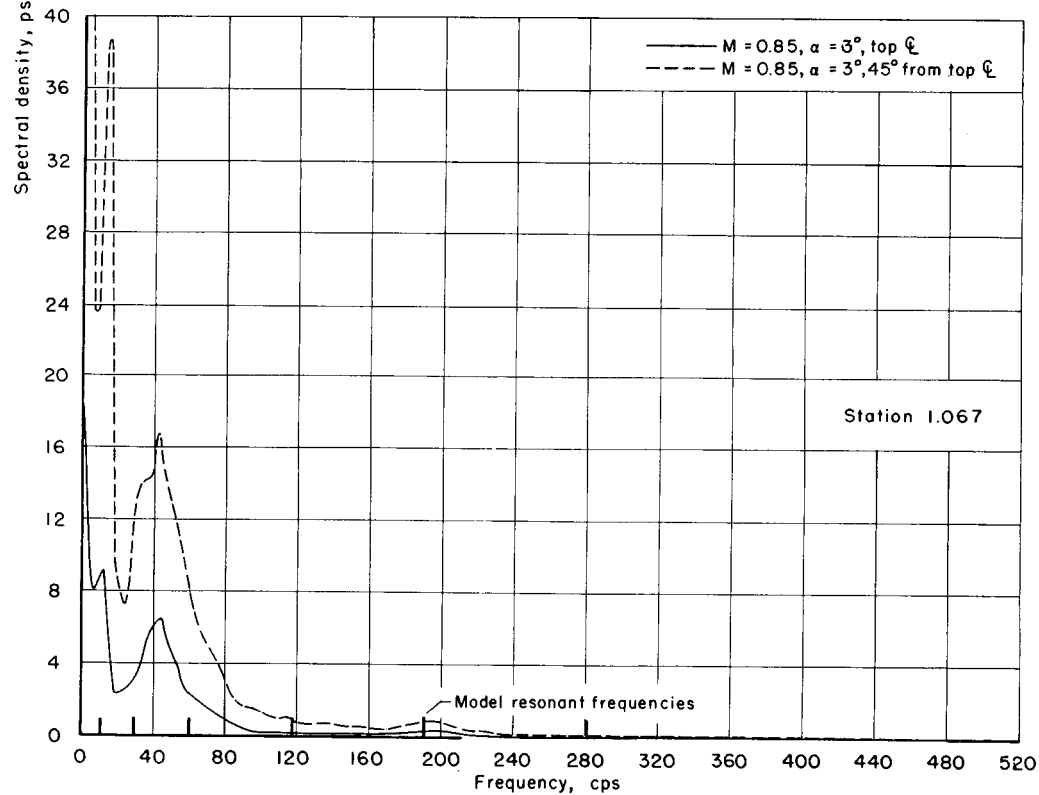
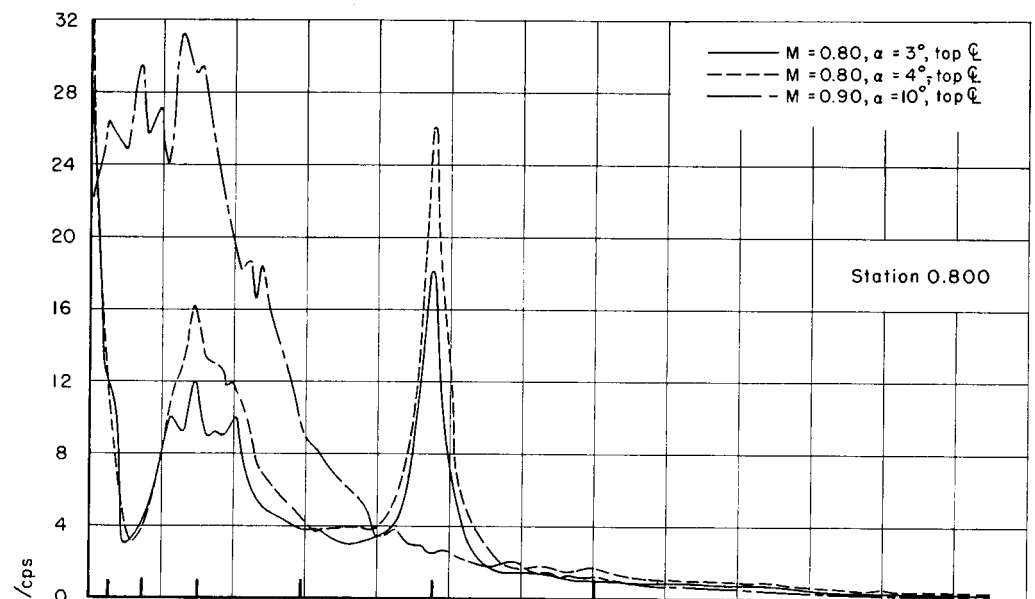
(a) Centaur model - Concluded.

Figure 14.- Continued.

DECLASSIFIED

CONFIDENTIAL

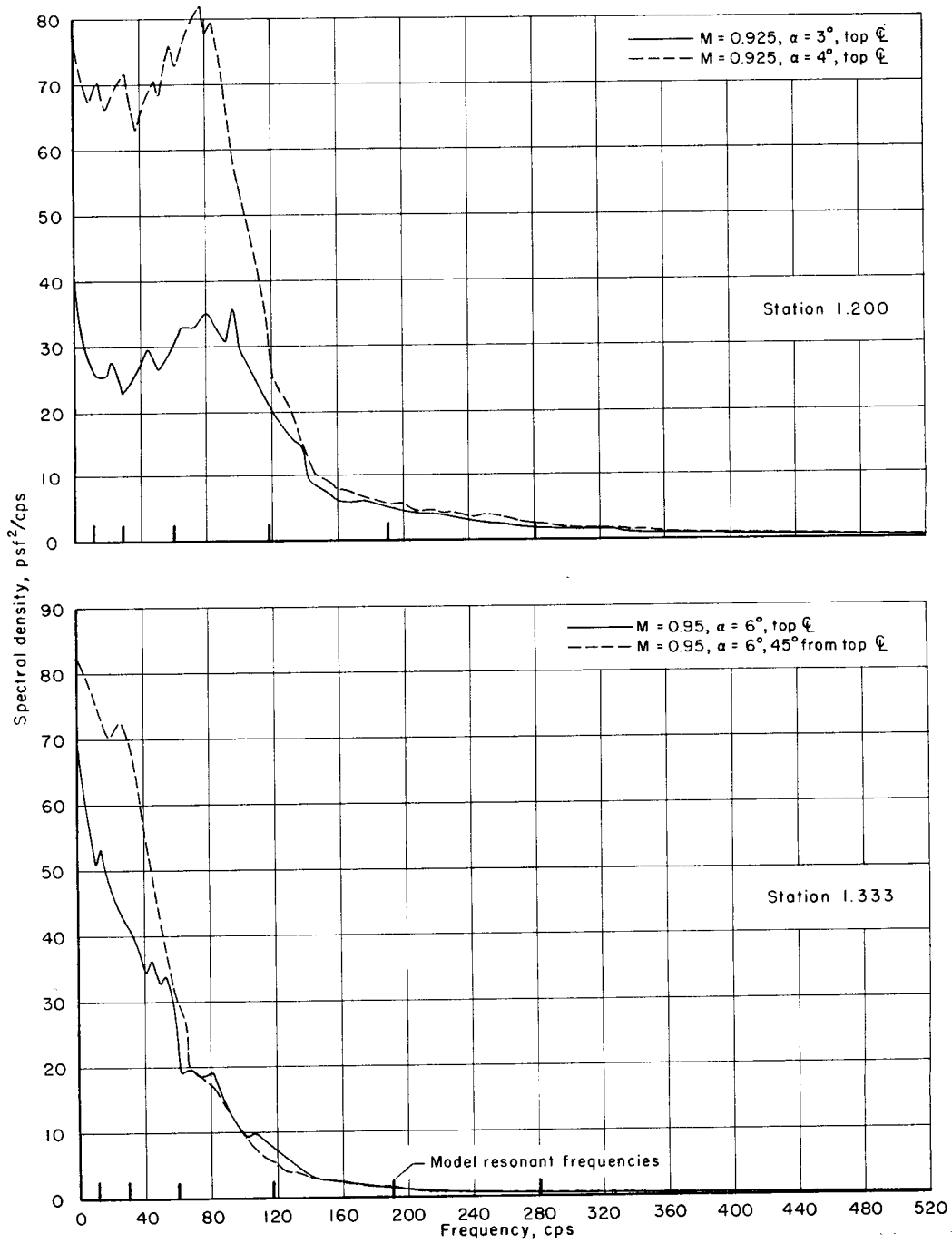
49



(b) Able-V model.

Figure 14.- Continued.

CONFIDENTIAL



(b) Able-V model - Concluded.

Figure 14.- Concluded.

DECLASSIFIED

CONFIDENTIAL

51

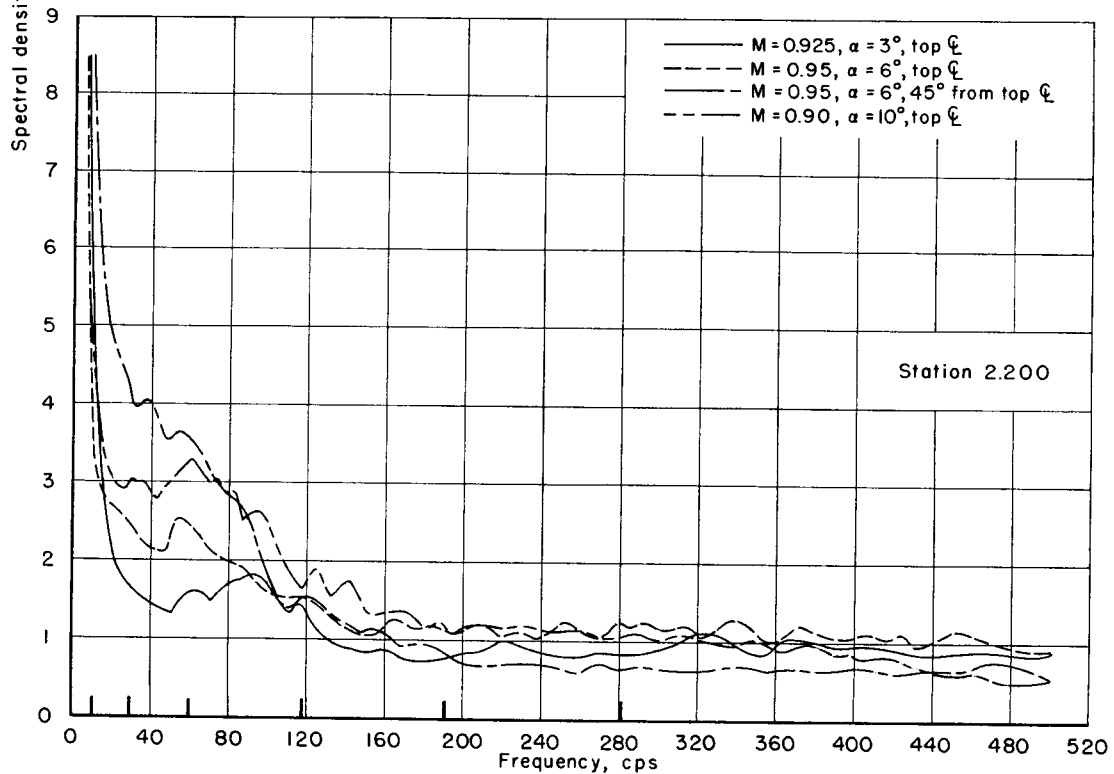
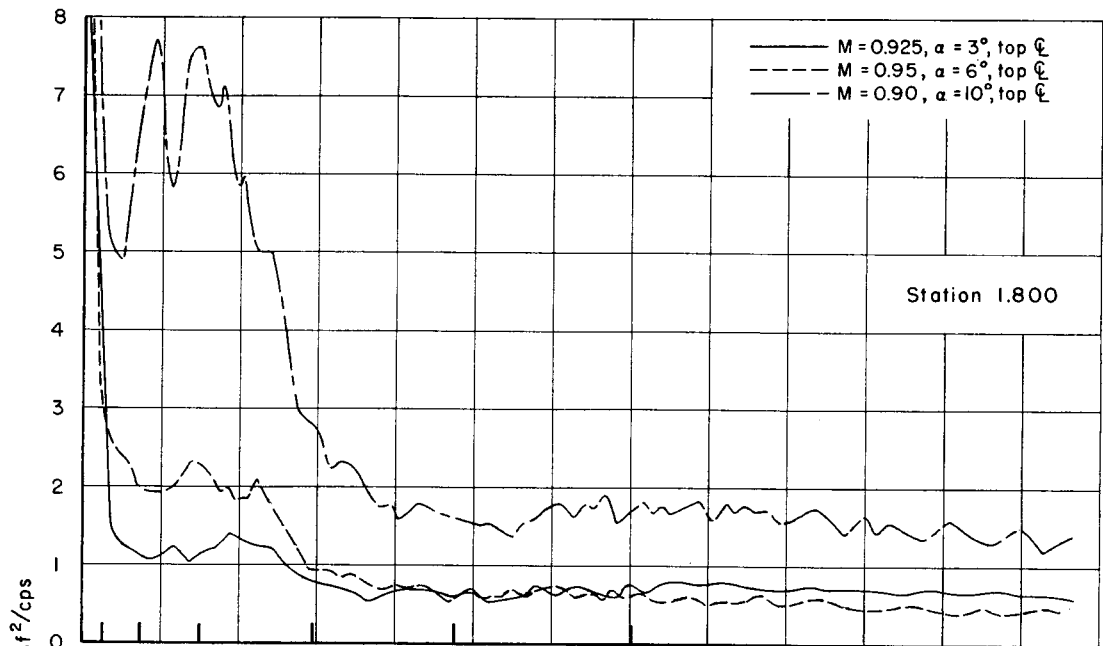


Figure 15.- Power spectral densities of pressure fluctuations on the Able-V model in the separated region following the shock wave.

03712301030

52

CONFIDENTIAL

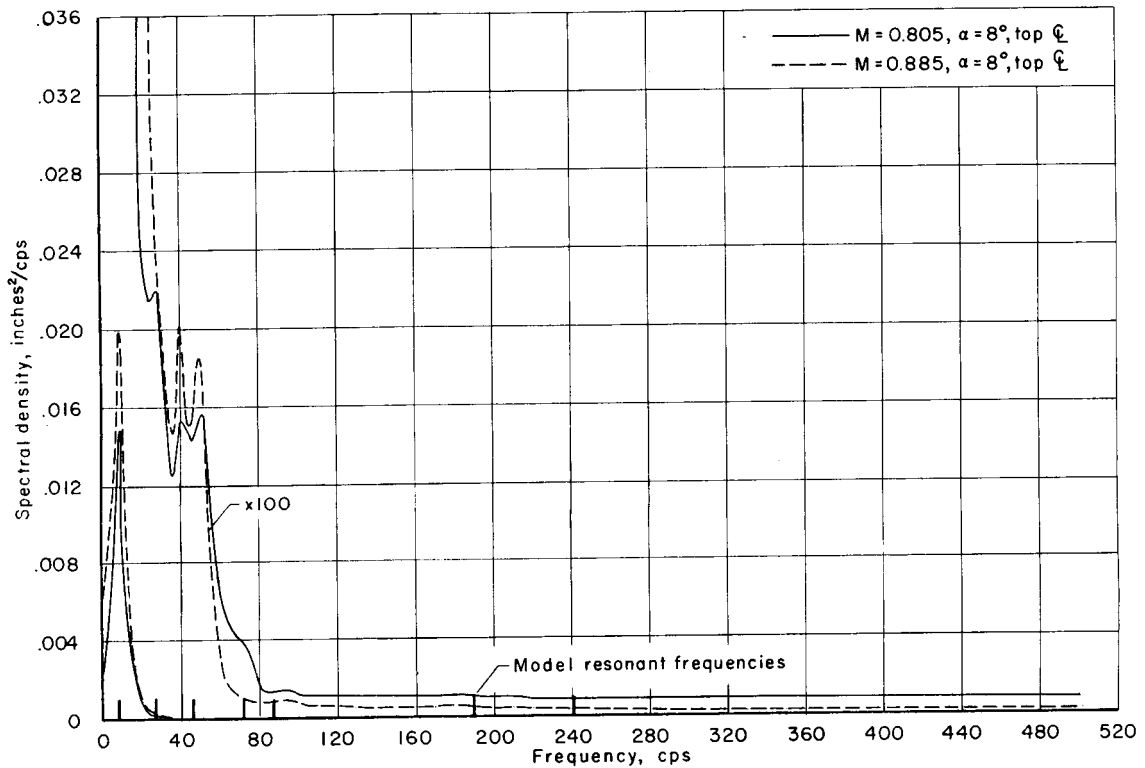


Figure 16.- Power spectral densities of amplitude of motion on the Centaur model.

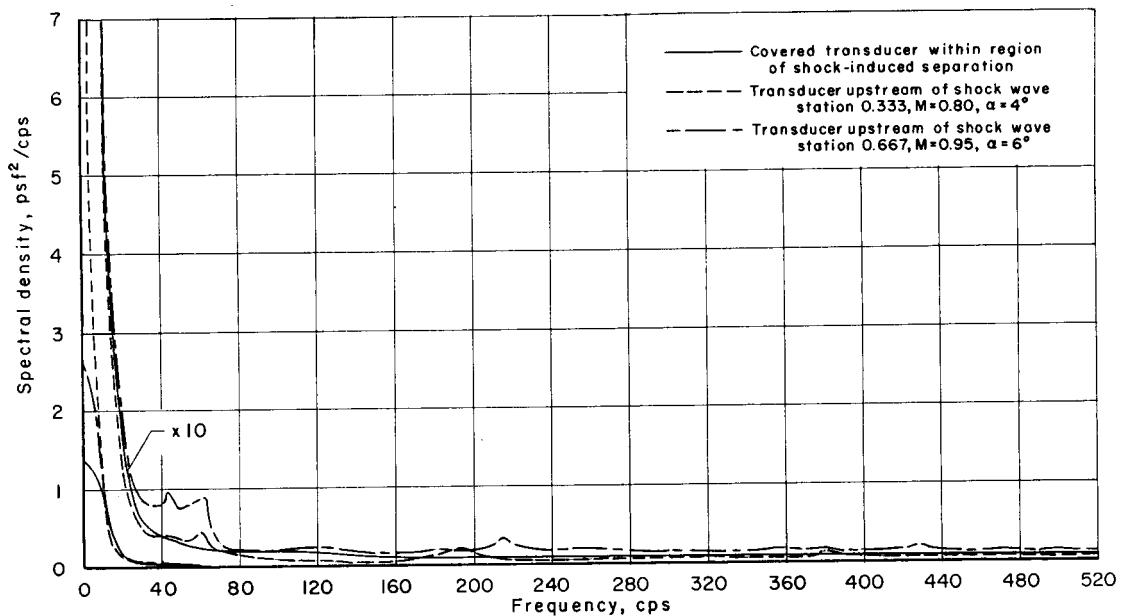


Figure 17.- Power spectral densities of response of a covered transducer and transducers ahead of the shock wave on the Able-V model.

DECLASSIFIED

CONFIDENTIAL

53

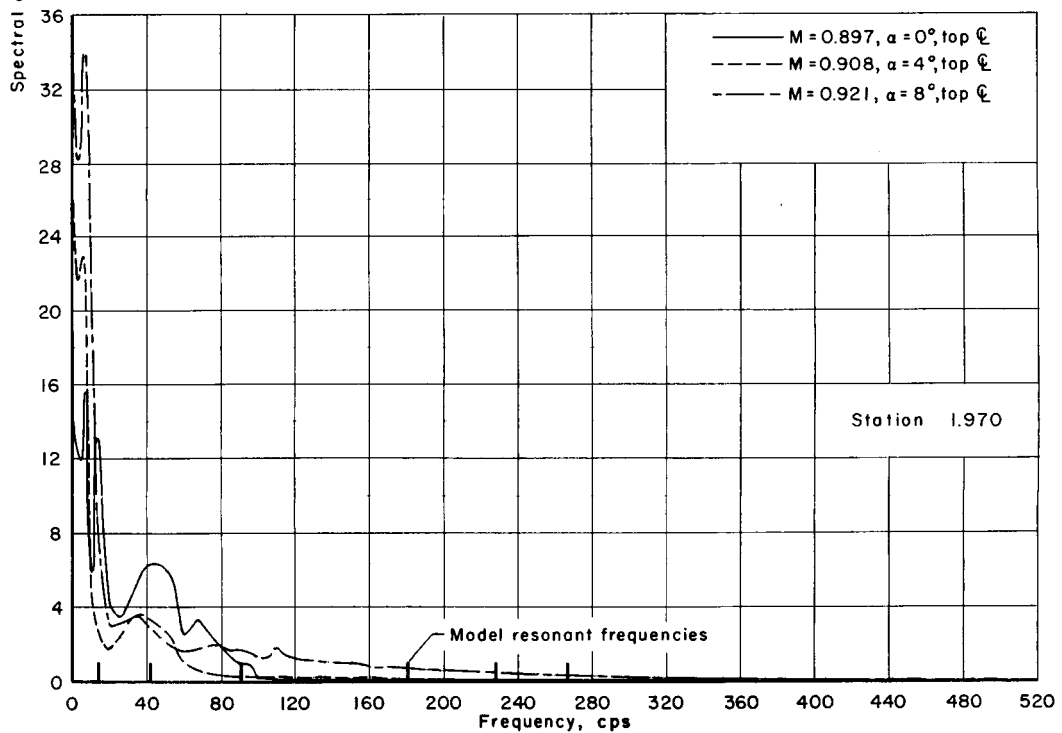
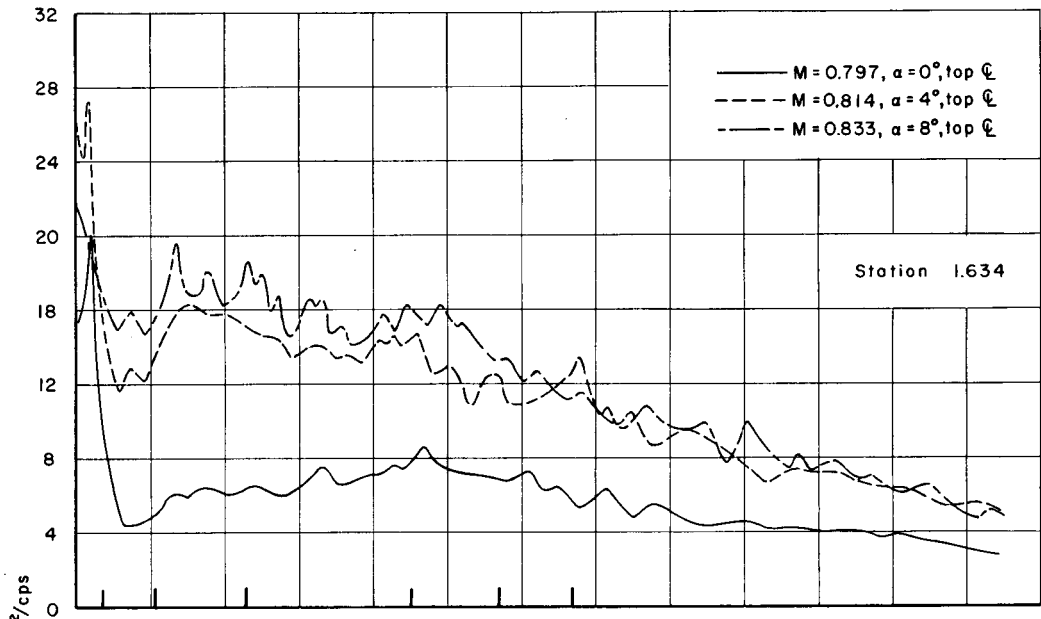


Figure 18.- Power spectral densities of pressure fluctuations at the normal shock wave on the Centaur model in the Ames 11-Foot Transonic Wind Tunnel.

031713281030

54

CONFIDENTIAL

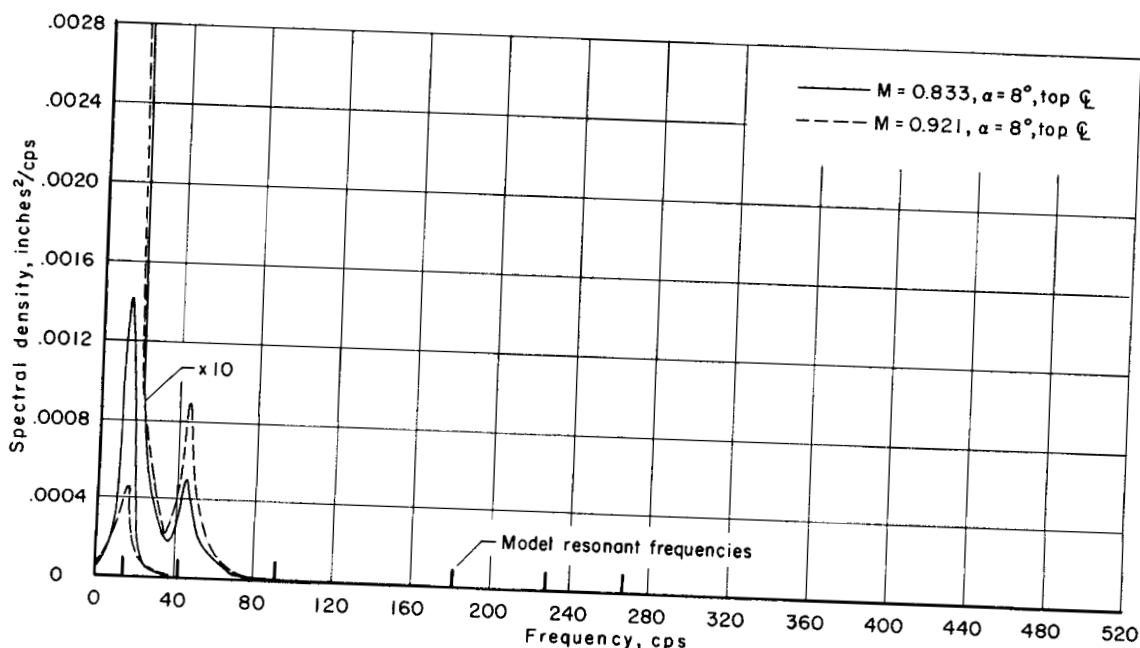


Figure 19.- Power spectral densities of amplitude of motion on the Centaur model in the Ames 11-Foot Transonic Wind Tunnel.

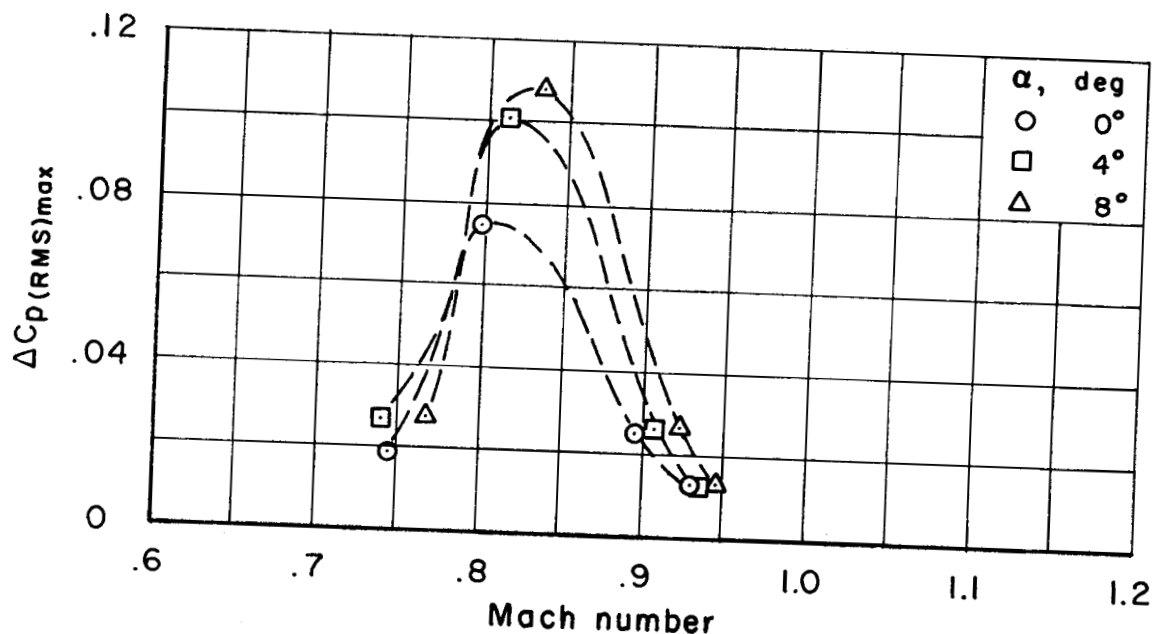


Figure 20.- The variation with Mach number of the maximum pressure fluctuations measured along the top center line of the Centaur model in the Ames 11-Foot Transonic Wind Tunnel.